Reliability analysis of timber structures considering variability in nonlinear joint behaviour

DOROTEA CAPRIO

Department of Architecture and Civil Engineering CHALMERS UNIVERSITY OF TECHNOLOGY Gothenburg, Sweden, 2025 Reliability analysis of timber structures considering variability in nonlinear joint behaviour

DOROTEA CAPRIO ISBN 978-91-8103-298-7

Acknowledgements, dedications, and similar personal statements in this thesis, reflect the author's own views.

© DOROTEA CAPRIO 2025 except where otherwise stated.

Selected material from the author's licentiate thesis: Dorotea Caprio, "Consideration of the non-linear behaviour of joints for efficient design of complex timber structures", Gothenburg, Sweden, April 2023, is republished in this Ph.D. thesis.

Doktorsavhandlingar vid Chalmers tekniska högskola Series number: 5756 ISSN 0346-718X

Department of Architecture and Civil Engineering Division of Structural Engineering Chalmers University of Technology SE-412 96 Gothenburg, Sweden Phone: +46 (0)31 772 1000

Cover:

The picture shows the multi-level approach on which the present work is based: the single-fastener joint level, the multi-fastener joint level and the structural level.

Printed by Chalmers Digital Printing Gothenburg, Sweden, October 2025

Errata corrige

Page	Location	Original	Corrected
Paper I, Page 13	Equation (7)	$\frac{\frac{\left(K_{in} - K_{p}\right)v}{\left(1 + \left(\frac{K_{in} - K_{p}}{F_{t}}\right)^{a_{1}}\right)^{1/a_{1}}} + K_{p}v$	$\frac{\frac{\left(K_{in}-K_{p}\right)v}{\left(1+\left(\frac{\left(K_{in}-K_{p}\right)}{F_{t}}\cdot v\right)^{a_{1}}\right)^{1/a_{1}}}+}{K_{p}v}$
Paper I, (Page 22, Page 23)	Figure 19 caption, Table 6 caption	"grade"	"degree"

Reliability analysis of timber structures considering variability in nonlinear joint behaviour

DOROTEA CAPRIO
Department of Architecture and Civil Engineering
Chalmers University of Technology

Abstract

In contemporary timber structures, joint behaviour is critical to overall performance and reliability. Yet joints are often idealised as pinned or rigid, despite their inherently nonlinear response. Current design rules prescribe a stiffness reduction ratio to account for the nonlinear behaviour. This simplification, coupled with the current component-based design checks, can misjudge structural reliability, leading to either unconservative or overly conservative design. This study aims to quantify the impact of the nonlinear behaviour of joints and related variability, specifically of steel-to-timber joints with selftapping screws, on the reliability of statically indeterminate timber structures. A multi-level probabilistic framework was implemented, taking into account three levels: single-fastener, multi-screw, and structural level. First, an empirical probabilistic model of single-screw joints was developed based on experiments conducted with different load-to-screw axis angles. This model was then used as input for a semi-analytical multi-fastener model based on a displacement-controlled equilibrium, which captured the moment-rotation curve and related variability of the multi-fastener joints. Finally, employing the Monte Carlo simulation method, a reliability analysis was conducted on a statically indeterminate timber beam. Uncertainties in loads, material and joints nonlinear behaviour were considered. Results indicated that applying the currently prescribed stiffness ratio in the design of beams with joints with laterally loaded screws led to a probability of failure nearly twice the target value, whereas beams with joints with inclined screws required no stiffness reduction to meet the target probability of failure. An optimisation algorithm was used to calibrate the stiffness reduction ratio, restoring the target probability of failure. The probabilistic framework presented herein can be applied to other structural systems and joint typologies for a safer and more rational design of modern timber structures.

Keywords: Reliability, indeterminate, timber, nonlinear, stiffness, ductility, system effects



List of Publications

[Paper I] D. Caprio, R. Jockwer, "Regression models for the description of the behaviour of modern timber joints."

Buildings, vol. 13, no. 11, Art. no. 2693, Nov. 2023. ISSN: 2075-5309. https://doi.org/10.3390/buildings13112693.

[Paper II] D. Caprio, R. Jockwer, "Experimental investigation and probabilistic modelling of the load-displacement behaviour of steel-to-timber joints with self-tapping screws."

Construction and Building Materials, vol. 489, Art. no. 141970, Aug. 2025. ISSN: 0950-0618.

https://doi.org/10.1016/j.conbuildmat.2025.141970.

[Paper III] D. Caprio, R. Jockwer, M. al-Emrani, "Reliability of statically indeterminate structures: modelling approaches and sensitivity study."

In: Current Perspectives and New Directions in Mechanics, Modelling and Design of Structural Systems, 2022, pp. 1649–1655.

ISBN: 978-1-003-34844-3.

https://doi.org/10.1201/9781003348443-270.

[Paper IV] D. Caprio, R. Jockwer, "Impact of steel-to-timber joints with screws on the failure modes and reliability of a structurally indeterminate timber beam."

Manuscript submitted for publication, 2025.

In **Paper I**, the author conducted the literature review, analyses and prepared all visualisations, and drafted and revised the manuscript (introduction, analysis, results and discussion, conclusions). The co-author of this paper contributed to the evaluation of the results and assisted in reviewing and editing the paper.

In **Paper II**, the author planned and carried out all experiments; developed the analytical model; performed the statistical analyses; conducted the literature review and prepared all visualisations, and drafted and revised the manuscript (introduction, analysis, results, discussion, conclusions). The coauthor of this paper contributed to the design and planning of the experiments, to evaluating the results and assisted in reviewing and editing the paper.

In **Paper III**, the author developed the analytical model, performed the statistical analyses, interpreted the results, prepared all visualisations, and drafted and revised the manuscript (introduction, analysis, results and discussion, conclusions). The co-authors of this paper contributed to the evaluation of the results and assisted in reviewing and editing the paper.

In **Paper IV**, the author planned and carried out all simulations; developed the probabilistic model, performed the statistical analyses, prepared all visualisations, and drafted and revised the manuscript (introduction, analysis, results and discussion, conclusions). The co-author of this paper contributed to the evaluation of the results and assisted in reviewing and editing the paper.

Other publications

In addition to the appended papers, the author has also written and contributed to the following publications:

- [a] R. Jockwer, D. Caprio, A. Jorissen, "Evaluation of parameters in-fluencing the load-deformation behaviour of connections with laterally loaded dowel-type fasteners."
 Wood Material Science & Engineering, vol. 17, no. 1, pp. 6–19, 2021.
 https://doi.org/10.1080/17480272.2021.1955297.
- [b] R. Jockwer, D. Caprio, "Reliability of complex timber structures: impact of connection nonlinearity and overstrength."
 14th International Conference on Applications of Statistics and Probability in Civil Engineering (ICASP14), Dublin, Ireland, Jul. 9–13, 2023.
- [c] D. Caprio, "Consideration of the non-linear behaviour of joints for efficient design of complex timber structures."

 Licentiate thesis, Chalmers University of Technology, Göteborg, Sweden, 2023.
 - $https://research.\ chalmers.\ se/en/publication/535125.$
- [d] D. Caprio, R. Jockwer, A. Ringhofer, "Parametrization of the non-linear behaviour of timber joints with self-tapping screws."
 In: Proceedings of the International Network on Timber Engineering Research (INTER), Meeting 57, Padova, Italy, 2024.

Contents

Αŀ	ostra	ct	i
Αc	knov	vledgements	хi
N	omen	ıclature	xiii
		Abbreviations	xiii
		Uppercase roman letters	xiv
		Lowercase roman letters	ιvii
		Uppercase greek letters	αviii
		Lowercase greek letters	ιviii
		Special characters	xix
ı	0	verview	1
1	Intr	oduction	3
	1.1	Background	3
	1.2	Aim of research	4
	1.3	Methodology	6
	1.4	Limitations	9
	1.5	Outline of the thesis	9

2	Stat	te of the art	11
	2.1	Background of current design methodology	11
	2.2	Design of the joint according to the standards	13
		Stiffness	13
		Ductility	15
	2.3	Load-displacement curve shapes in timber joint	16
		Joints with bolts and dowels	16
		Glued-in rods	17
		Self-tapping screws	18
	2.4	Modelling of timber joints	21
		Mathematical models	21
		Analytical and semi-analytical models	23
		3D and 2D FEM models	32
	2.5	Statically indeterminate structures	32
		Portal frames	32
		Continuous floors	34
		Arches and trusses	34
		Gridshells and domes	35
	2.6	Reliability analysis	36
		Methods of structural reliability	36
		Reliability of systems	40
		Reliability studies on timber structures	42
3	Ana	llysis	45
	3.1	The case study	45
		Design of the structure	46
	3.2	Model for single-screw joint	48
		Experimental investigation	48
		Empirical-probabilistic modelling	51
	3.3	Model for multi-screw joint	54
	3.4	Model for moment-rotation curve	54
	3.5	Reliability analysis of the structure	54
4	Res	ults and discussion	59
	4.1	Design of the structure	59
	4.2	Single-screw joint model	60
		Selection of the mathematical model	60

		Empirical-probabilistic model	62
	4.3	Multi-screw joint model	64
	4.4	Reliability analysis of the structure	65
		Methodology selection	
		Full reliability analysis	67
5	Con	clusions and future work	7 1
	5.1	Conclusions	71
		General conclusions	71
	5.2	Future work	76
Α	Loa	d-displacement curves	79
Re	ferer	nces	83
11	Pa	pers	93
I			11
II			111
Ш			1111
IV			IV:

Acknowledgments

The work presented in this thesis was conducted at the Division of Structural Engineering at Chalmers University of Technology between October 2020 and September 2025. The research project was funded by Svensk Trä, the Swedish association of the timber industries, and TMF, the Swedish Federation of Wood and Furniture Industry, to which the author expresses her gratitude.

"Los metafísicos de Tlön no buscan la verdad ni siquiera la verosimilitud: buscan el asombro." — Tlön, Uqbar, Orbis Tertius (in Ficciones), Borges. For me, doing a PhD, and doing science, has been an act of wonder, a practice of discovery. I want to thank my supervisors, Prof. Robert Jockwer and Prof. Mohammad al-Emrani, for believing in me back in 2020 and encouraging me to pursue a PhD. I always tried to honour this with commitment and perseverance, in particular during the challenging moments of the PhD journey. None of this work could have been possible without your mentorship. It is impossible not to mention my examiner, Prof. Karin Lundgren, whose advice and feedback further improved my work.

I'm one of those people who often wonder about the past, what could have been, the persistent what if. I sometimes forget to enjoy the present and focus on the now. In structural engineering, that tendency toward abstraction can seem negative; for a long time, I doubted I'd fit in the field. Yet that very contrast is what drew me in: stepping out of my comfort zone while still honouring my abstract leanings. Engineering also demands attention to the tangible materials, structures, physical space, and how things come together. For me, that's an invitation to live in the present moment. Engineering has become my daily practice of presence. This became particularly true at the laboratory at Chalmers during testing. Conducting experiments demanded full presence: attention to instruments, specimens, and safety.

I'm grateful to Senior Research Engineers Sebastian Almfeldt and Anders Karlsson for helping me prepare the tests and navigate the lab. I also thank my former undergraduate students, Nicklas Vallström and Olle Dahlberg, for their assistance with parts of the laboratory experiments.

I would also like to thank all my colleagues and peers at the Division of Structural Engineering for all the shared lunches and fika. I would also like to thank my family and friends from Italy. Leaving you behind was not easy, but you always supported me.

L'ultimo ringraziamento va al mio fidanzato e futuro marito Daniele. Quando

penso a noi, non mi viene in mente nessuna citazione pretenziosa, solo parole semplici. Allora voglio dirti semplicemente *grazie*, perché con la tua presenza regali profondità a tutte le mie azioni, compresa quest'avventura del PhD. Non vedo l'ora di sposarti il prossimo Maggio e iniziare il prossimo capitolo dell'esistenza insieme.

Gothenburg, Sweden Tuesday 30th September, 2025

 $Dorotea\ Caprio$

Nomenclature

Abbreviations

CLT Cross-laminated timber.
CoV coefficient of variation.
DTF dowel-type fasteners.
DIC digital image correlation.

EC5 Eurocode 5. EC8 Eurocode 8.

FEM Finite element model.

FORM First Order Reliability Method.

GiR Glued-in rod(s).

GL Glued laminated timber. IS Importance Sampling.

JCSS Joint Committee of Structural Safety.

LVL laminated veneer lumber.
 MCS Monte Carlo Simulation.
 PCE Polynomial chaos expansion.
 PDF Probability density function.
 SLS Serviceability limit state.

SORM Second Order Reliability Method.

ST solid timber.

STS Self-tapping screws. Subset Subset Simulation.

TCC Timber Concrete Composite.

ULS Ultimate limit state.

Uppercase roman letters

 A_I Cross-sectional area of the inner member (Lantos

model).

 A_m Cross-sectional area of the wood member (Wilkinson

model).

 A_O Cross-sectional area of the outer member (Lantos

model).

 A_n Cross-sectional area of one steel side plate (mm²).

 A_s Nominal threaded area of a rod.

 A_s Cross-sectional area of the steel plate (Wilkinson

model).

 C_1, C_2 Reduction factors for the first and last fastener

(Cramer model).

 C_g Group-action factor in NDS-2024. $D_{ab,max}$ Absolute ductility at maximum.

 $D_{ab,u}$ Absolute ductility at failure.

 D_f Failure domain.

 $D_{r,max}$ Relative ductility at maximum. $D_{r,u}$ Relative ductility at failure.

 E_b Elastic modulus of bolt (Cramer model).

 E_{beam} Elastic modulus of wood.

 E_I Elastic modulus of wood, inner member (Lantos

model).

 $E_{m,beam}$ Mean value of the elastic modulus of wood.

 E_{O} Elastic modulus of wood, outer member (Lantos

model).

 E_p Elastic modulus of the steel plate (Cramer and

Wilkinson model).

 E_w Elastic modulus of wood (Cramer Model). F Total external applied load (Cramer model).

 F_a Asymptotic load level approached for large displace-

ments (Glos model).

 F_{est} Estimated load-carrying capacity.

 $F_{exp,j}$ Experimental loads vector at the jth increment. F_{max} Maximum load (peak force) on the curve.

 $F_{multi,i}(\Delta_{v,i})$ Load carried by the entire multi-screw joint at dis-

placement level i (N).

 $F_{multi.i}$ Load carried by the multi-screw joint at displacement

step i.

 $F_{single,j}(\Delta_{v,i})$ Load carried by the j-th individual screw at displace-

ment level i.

 F_t Force intercept of the plastic tangent (Foschi and

Richard-Abbott models).

F(v) Load as a function of displacement v.

 F_i Failure event of component i.

 F_i^c Survival (complement) event of component i. $F_{t,0.95}$ 95th -percentile tensile capacity of the joint (N). $F_{w,k}$ Characteristic value of withdrawal capacity (N). I_b Moment of inertia of bolt (Cramer model).

 I_{beam} Moment of area of the beam cross-section. I_p Moment of inertia of plate (Cramer model).

 K_{10-40} Elastic secant stiffness.

 K_{in} Initial elastic stiffness (Foschi and Richard-Abbott

models).

 K_{max} Tangent stiffness at the point of maximum load (Glos

model).

 K_p Plastic (post-yield) stiffness of the curve (Foschi and

Richard-Abbott models).

 $K_{\theta,joints}$ Rotational stiffness of the joints. K_{SLS} Serviceability limit state stiffness.

 K_{SLS} Lateral stiffness of the single-fastener joint at the SLS. $K_{SLS,ax}$ Axial stiffness of the single-fastener joint at SLS. Shear stiffness of single-fastener joint at SLS.

 K_{ULS} Ultimate limit state stiffness.

 $M_{E,\max}$ Design bending moment along the beam. $M_{Ed,field}$ Design bending moment at midspan. $M_{Ed,joints}$ Design bending moment at the joints.

 $M_{R,joints,i}$ Bending resistance of joints at displacement incre-

ment i.

 M_{tor} Value of the applied torque in the experiments. $M_{tor,k}$ Characteristic torsional moment of the screw. $M_{y,k}$ Characteristic yield moment of the screw (N·m).

N Number of samples. N_f Number of failures.

 $P_{F,i}$ Lateral force transferred by fastener i (Lantos model).

 P_{HTO} Probability of head-tear-off failure. P_i Force carried by bolt i (Cramer model).

 $P_{I,i}$ Force in the inner member just after fastener i (Lan-

tos model).

 P_{max} Maximum lateral load applied to the joint (Lantos

model).

 $P_{O,i}$ Force in the outer member just after fastener i (Lan-

tos model).

 P_{single} Capacity of single-fastener (Lantos model).

 P_{ii}^* Load carried by timber member between fastener i

and timber branch j (Wilkinson model).

 P_{WITH} Probability of withdrawal failure.

 P_f Probability of failure.

 p_i Failure probability of component i. \widehat{P}_f Expected value of probability of failure. $P_{f,parallel}$ failure probability of a parallel system. $P_{f,series}$ failure probability of a series system.

 R^2 Determination coefficient.

S Centre-to-centre spacing between adjacent fastenerst

(Lantos model).

 K_p Axial compliance factor of the steel plates (Cramer

model).

 K_w Axial compliance factor of the wood (Cramer model). Y_{ji} Tangent tiffness for fastener i on branch j (Wilkinson

model).

Lowercase roman letters

 a_1 Shape parameter (Richard-Abbott model).

 b_{beam} Width of the timber beam. c_1, c_2, c_3, c_4, c_5 Coefficients of the Glos model. d Diameter of the fastener.

d Nominal (outer) diameter of the screw.

 d_{core} Core diameter of the screw.

 f_m Bending strength of the timber material. $f_{m,d}$ Design value of the bending strength.

 $f_{tens,k}$ Characteristic value of the tensile capacity of the

screw.

 $f_{tens,k,exp}$ Characterstic value of the tensile capacity of the

screw measured in experiments.

 $f_{tens,m,exp}$ Mean value of the tensile capacity of the screw mea-

sured in experiments.

 $f_{y,0.95}$ 95th-percentile yield strength of the rod material.

g Performance function. h_{beam} Height of the beam section.

k Foundation modulus (Cramer model).

 k_f Foundation modulus of wood (Cramer model).

 k_1, k_2, k_3, k_4 Coefficients of the Brandner model.

 $k_{m,i}$ Elastic stiffness of the wood (Wilkinson model). k_s Elastic stiffness of the steel plate (Wilkinson model).

 l_{screws} Self-tapping screws length. l_{eff} Effective length of the screw).

 $m_{1,2}$ Roots of the characteristic equation of the difference

system (Lantos model).

 n_{screws} Number of equally spaced fasteners.

 n_{HTO} Number of specimens that failed by head-tear-off.

 n_{tot} Total number of tested specimen.

 n_f Number of fasteners (Lantos and Cramer models). r Centre-to-centre spacing between bolts (Wilkinson

model).

 t_p Thickness of one steel side plate (Cramer model).

t_w	Thickness of the wood member (Cramer model).
v_{max}	Displacement at load-carrying capacity F_{max} .
v_u	Ultimate displacement.
v_y	Displacement at yielding.
x_N	Length of neutral axis mesured from the compression
	side.
y	Total deformation of the bolt (Cramer model).
y_b	Elastic slip of a bolt against a steel plate (Cramer
	model).
y_e	Elastic slip of a bolt in the wood (Cramer model).
z	Lever arm between the screw row and the rotation
	point.

Uppercase greek letters

 Δ_i Displacement of fastener i (Lantos model).

 $\Delta_{v,i}$ Displacement at i^{th} load increment in the multi-screw model.

Lowercase greek letters

α_{group}	Group-efficiency factor (Lantos model).
α	Multiplication factor for moment at joints.
β	Multiplication factor for moment at midspan.
β_c	Magnification factor (Cramer model).
β_{rel}	Target reliability index.
δ_{ji}^*	Displacement at the branch-transition point for fas-
J	tener i on branch j .
γ	Load-to-screw axis angle.
γ_f	Stiffness of a single-fastener (Lantos model).
μ	Coefficient of friction between the connected mem-
	bers.
ω	Dimensionless joint-stiffness parameter (Lantos
	model).
ϕ	Standard normal cumulative distribution function.

 ψ Ratio between the stiffness of wood and steel plate (Cramer model).

 Φ Dimensionless slip-to-axial-stiffness ratio (Lantos model).

 ρ Correlation coefficient. ρ_{den} Density of the timber.

 ρ_m Mean density of the timber member. θ_i Rotation of the joint at load step i.

 ε_I Axial strain in the inner timber member (Lantos model).

 ε_O Axial strain in the outer timber member (Lantos model).

Special characters

C Correlation matrix of the random variables.

 $\begin{array}{ll} \boldsymbol{\Delta v} & \text{Vector of displacement at the joints.} \\ \boldsymbol{F}_{multi} & \text{Vector of the forces at the joint.} \\ \boldsymbol{K} & \text{Stiffness matrix of the joint.} \end{array}$

L Cholesky factor of C.

M Vector of material parameters.

 \mathcal{N} Normal distribution.

 $\mathcal{O}(\cdot)$ Landau big-O notation (order term).

 \widehat{P}_f Estimator of the probability. \mathbf{P}_{mod} Vector of the models parameter.

P Probability measure.

 $\sigma_{\widehat{P}_f}$ standard deviation of the estimator \widehat{P}_f .

X Vector of independent standard-normal random variables

 \mathbf{X}_{corr} Vector of correlated random variables ($\mathbf{X}_{corr} = \mathbf{L}\mathbf{X}$). \mathbf{X}^{enr} Candidate enrichment point added to the experimental design (vector of input variables).

Part I Overview

CHAPTER 1

Introduction

1.1 Background

"A structure is a constructed assembly of joints separated by members" (McLain [1]). This statement perfectly applies to timber structures, since joints¹ represent the most challenging and costly element of timber construction, requiring a lot of material and production resources [3]. During the last years, large-span, tall timber structures have been built around the world as never before. In these new applications, joints have become the key elements in design: they must permit disassembly for reuse, provide acoustic isolation, and supply the ductility needed for energy dissipation under seismic or dynamic loading. Nevertheless, according to the current design rules, joints are modelled as linearly elastic, while reliable information on ultimate rotations and displacements is lacking. Misjudging these properties can lead (and has led) to structural failures in modern timber structures [4]. Moreover, the design

¹The terms 'joint' and 'connection' are often used as synonyms in the literature. In [2] the connection is defined as the union of two or more joints, and the joint is defined as an ensemble of fasteners with two or more members. In this paper, the joint is used for both cases for simplicity's sake.

of the overall structures is based on a component-by-component approach: the capacity of each component of the structure is checked against the load effects, applying the so-called partial safety factors [5]. System effects at the component level (at the joint level) and structural level (between the members and the joints) are therefore almost totally dismissed. Previous reliability and numerical analyses showed how incorporating nonlinearities that characterise the load-displacement curve of joints affected the load distribution of forces in timber structures [5]–[7].

Various issues are to be analysed in more detail so as to better predict the reliability of modern timber structures. The following points were concluded to be of particular interest:

• Representation of the nonlinear behaviour of joints and the related variability.

Currently, Eurocode 5 (EC5) considers the nonlinear behaviour of joints in a simplistic way, by reducing the stiffness at the ultimate limit state K_{ULS} to 2/3 of the stiffness at the serviceability limit state K_{SLS} . However, this ratio is based on experimental data on nailed joints in the 1960s [8]–[10], and it can be inadequate to cover all the joint typologies and design situations.

• Consideration of system effects in the structure.

The common approach, component-by-component check, can be adequate for traditional light wood structures, but is unsuitable for more complex ones. A structure must be analysed as a system of interconnected elements that interact with each other [5].

Neglecting the actual nonlinear behaviour of joints and, at the same time, adopting a component-by-component approach might lead to an underdesign or overdesign of the complex timber structure at the ultimate limit state (ULS).

1.2 Aim of research

This thesis aims to quantify the impact of nonlinear behaviour of joints and their variability on the reliability of modern timber structures. For this aim, a relevant structural system and joints were selected.

Choice of structure.

This thesis adopts a statically indeterminate timber beam as its case study because, in statically indeterminate structures, the internal force distribution is dictated by both equilibrium and compatibility, making joint nonlinear load-displacement behaviour critical. A statically indeterminate beam represents the simplest member of more complex statically indeterminate structures and it is common in practice, particularly in glulam (GL) portal halls. Its prevalence and structural simplicity make it a representative structure for the present thesis.

Choice of joint type.

Joints with self-tapping screws (STS) can present a variety of load-displacement shapes. Therefore, choosing this type of joint allowed a systematic exploration of how different curve "shapes" affect the reliability of the structure.

Examples of statically indeterminate structures with joints with self-tapping screws are present in reality in multiple applications [11]–[13].

Consequently, the study of a statically indeterminate timber beam with steel-to-timber joints with self-tapping screws offers a representative example to get insights into how joint nonlinearity influences internal force redistribution and overall reliability. Based on these motivations and choices, this thesis addresses the following research questions:

- (i) **RQ1** (Single-screw joint level): How to model the nonlinear behaviour and the variability of a single-screw joint as a function of the selected influencing parameters?
- (ii) RQ2 (Multi-screw joint level): How can the nonlinear behaviour and the variability of a multi-screw joint be modelled using the empirical probabilistic model of a single-screw as input? How should the momentrotation curve be derived?
- (iii) RQ3 (Structure level): How does the probabilistic nonlinear behaviour and variability of joints affect the reliability of a statically indeterminate beam, and are existing design rules sufficiently reliable?

1.3 Methodology

The methodology follows a bottom-up multi-level approach according to which the structure is analysed at three levels: the single-screw joint, the multi-screw joint and the structural level.

At the single-screw joint level, the output was a probabilistic model to describe the nonlinear displacement curve of single-screw joints. To achieve this, two inputs were required: an analytical model and experimental data. A review of existing mathematical models was conducted, and the model with the best accuracy and description of the load-displacement curve variability was selected. Then, the experiments provided the load-displacement data of single-screw steel-to-timber joints. Each coefficient of that model was then treated as a random variable, and their correlations were estimated, giving a fully probabilistic description of the load-displacement curve of a single-screw joint.

Because joints in real structures employ groups of screws, the next level is represented by the multi-screw joint. The empirical-probabilistic model of the single-screw joint was used as input in the multi-screw joint model. An incremental displacement-controlled semi-analytical approach was used to obtain the overall load-displacement curve for a multi-screw joint.

Finally, the last level is the structural one. A statically indeterminate timber beam was designed in accordance with EC5, and each joint was modelled with nonlinear moment-rotation curve. A reliability analysis of the structure gave information on how the joints nonlinear behaviour affected the probability of failure. Design recommendations for the ratio for the design of joints with screws at ULS were given in order to meet the target probability in design.

The multi-level methodology is illustrated in Figure 1.1 and in Figure 1.2.

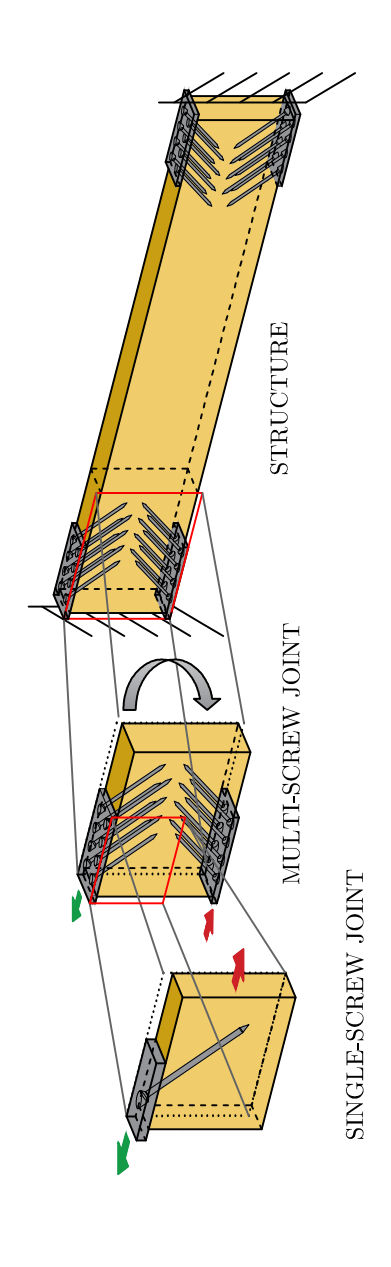


Figure 1.1: Multi-level approach. Three levels are considered: the single-screw joint, the multi-screw joint, and the structure.

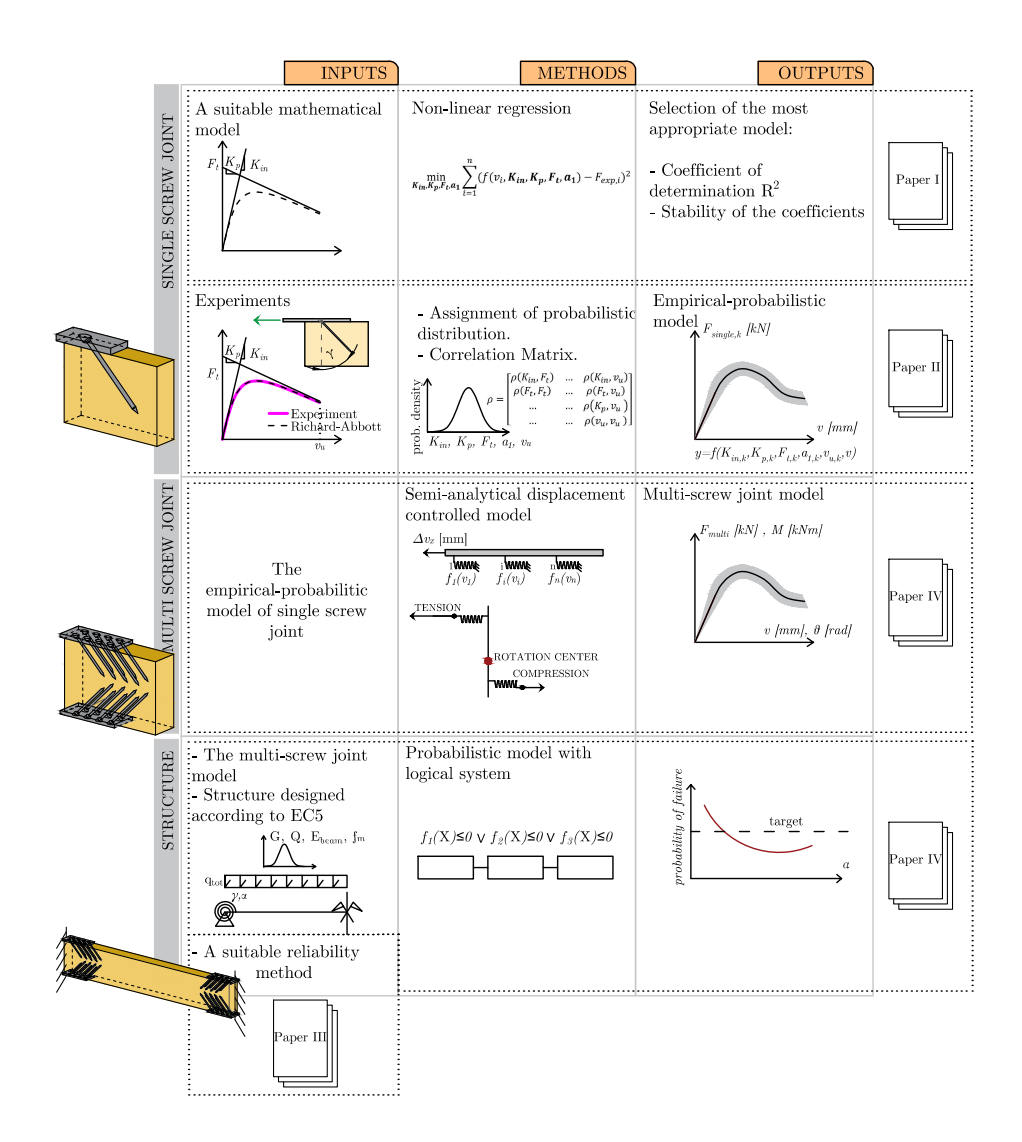


Figure 1.2: Overview of the workflow used in this thesis.

1.4 Limitations

The present thesis has the following relevant limitations:

- (i) The number of test repetitions per configuration used to characterise the load-displacement behaviour of single-screw joints was limited; additional data are required to validate the observed trends. The validity of the model cannot be demonstrated for other joint configurations with material and geometrical properties outside the range of those that have been adopted and tested.
- (ii) The multi-screw model assumes the adopted spacings were sufficient to avoid interaction effects. The assumption might be inadequate if spacing is reduced and a small spacing is adopted between the screws.
- (iii) The calibrated ratio K_{ULS}/K_{SLS} was established under specific assumptions about the multi-screw joint and its moment-rotation behaviour. Consequently, the ratio is only valid within the framework of those assumptions, and its applicability beyond them has not been demonstrated.
- (iv) In the reliability analysis, only the bending failure of the beam was considered; other potential failure modes (e.g., shear, local buckling) and their interactions were not addressed.
- (v) Potential brittle failure modes (such as net-tension failure, block-shear, and plug-shear, etc) and their impact on the reliability of the examined structure were also not studied.
- (vi) The analysed structural system (statically indeterminate timber beam) provides an insight into the reliability of the more complex structural system. However, it represents only a part of the real, more complex structure composed of many members and joints.

1.5 Outline of the thesis

This thesis consists of an introductory part and four appended papers. The former is divided into five chapters:

Chapter 1 provides the background of the work, and it explains the aim, the methodology, and the limitations of the thesis. This section positions **RQ1–RQ3** within a broader thesis aim and outlines the overall methodology along with its limitations.

Chapter 2 provides a comprehensive overview and expands on the background underlying **RQ1**– **RQ3**. In particular, it examines current design approaches, design rules for joints, experimental studies on timber joints, examples of applications of statically indeterminate timber structures, and techniques for estimating the reliability of structures.

Chapter 3 provides the methods used for each level of the three-level framework. First, it illustrates how the design of the case study structure was conducted, then it describes the development of the empirical-probabilistic model of the single-screw joint (**RQ1**); second, of the multi-screw joint model (**RQ2**); and third, of the probabilistic model of the structure (**RQ3**).

Chapter 4 provides the key findings of the multi-level framework. It first illustrates the results from the design of the case study structure, then the empirical-probabilistic model for single and multi-screw systems (**RQ1** and **RQ2**), followed by the methodology and reliability analysis outputs (**RQ3**).

Chapter 5 summarises the main conclusions of the present thesis and gives suggestions for future research.

CHAPTER 2

State of the art

This chapter presents the theoretical background and aligns with the multilevel framework. It opens with a brief overview of the current design methodology in Section 2.1. The discussion then moves from joint level to structural level. Sections 2.1–2.4 review both single- and multi-fastener design and modelling approaches, providing essential background for RQ1 and RQ2 and supporting Paper I and Paper II. Following this, Sections 2.5 and 2.6 address the structural level by examining statically indeterminate applications and reliability methods respectively, thereby expanding the background for RQ3 and supporting Paper III and Paper IV.

2.1 Background of current design methodology

Structural design is a decision-making process carried out under uncertainty [14]. Sources of uncertainty include, among others, material resistance, applied loads, joint behaviour or mathematical models. These uncertainties are typically classified as either aleatory or epistemic [15], [16]. Aleatory uncertainty stems from inherent natural variability, whereas epistemic uncertainty arises from the simplifications and incomplete knowledge embedded in the

mathematical models used to represent the physical system. Guidance on the design and the verification of structures under these uncertainties is provided in ISO 2394 [17]. In ISO 2394 [17], three different decision methods are described, which differ according to the level of detail with which the design or verification is performed.

The risk-informed decision has the highest level of detail (Level 4). In this case, the decision-making process considers both the safety and economic consequences, as well as explicitly models the associated uncertainties. Due to its complexity and time requirements, this approach is rarely implemented in routine practice and only reserved for exceptional cases. A less complex alternative is represented by a reliability-based decision (Level 3). At this level, the consequences are not explicitly taken into consideration; however, the design of the structure is conducted to achieve a certain target reliability. The chosen target reliability (β_{rel}) depends on the consequences and the type of structure. For example, according to the Joint Committee of Structural Safety (JCSS) [18], the probability of failure (P_f) and the related β_{rel} is associated with certain consequences and the cost of safety measures for a reference period of one year (Table 2.1).

Table 2.1: Target reliability index (and associated target failure probabilities) related to a one-year reference period ULS [18]

Cost	Minor consequences	Moderate consequences	Large consequences
High	$\beta_{rel} = 3.1 \ (\approx P_f = 10^{-3})$	$\beta_{rel} = 3.3 \ (\approx P_f = 10^{-4})$	$\beta_{rel} = 3.7 \; (\approx P_f = 10^{-4})$
Normal	$\beta_{rel} = 3.7 \; (\approx P_f = 10^{-4})$	$\beta_{rel} = 4.2 \ (\approx P_f = 10^{-5})$	$\beta_{rel} = 4.4 \; (\approx P_f = 10^{-5})$
Low	$\beta_{rel} = 4.2 \; (\approx P_f = 10^{-5})$	$\beta_{rel} = 4.4 \ (\approx P_f = 10^{-5})$	$\beta_{rel} = 4.7 \; (\approx P_f = 10^{-6})$

Finally, the semi-probabilistic approach corresponds to the lowest level of detail (Level 1). The semi-probabilistic approach relies on the fulfilment of the safety deterministic criteria, for which the effects of loads must be less than the resistance of the structural system. This translates into the use of partial safety factors, which are usually applied to resistance and loads, which have been previously calibrated in order to meet the prescribed reliability requirements. This approach is proposed by several national and international design standards, such as the Eurocodes (CEN EN1990 2002 [19]), when dealing with common situations in terms of uncertainties and consequences. An overview of the discussed approaches and levels of decision-making is illustrated in Table 2.2.

Table 2.2. Different revers of decision making according to 150 2504 [11]				
Approach	Application	Goal	References	
Risk-informed	Exceptional	Minimisation of	ISO 2394	
Risk-illiorined	design situations	consequences	150 2594	
Reliability-based design	Unusual	Reliability	JCSS	
Renability-based design	design situations	requirements	JOSS	
Semi-probabilistic	Usual	Deterministic design	Semi-probabilistic	
Seim-probabinstic	design situations	criteria	design codes	

Table 2.2: Different levels of decision making according to ISO 2394 [17]

2.2 Design of the joint according to the standards

Stiffness

EC5 [20] provides equations to determine the stiffness at SLS $K_{SLS,v}$ for joints with laterally loaded dowel-type fasteners (DTF), in dependency of the mean value of the density and of the (nominal) diameter d of the fastener. The stiffness formula differs for the type of fastener considered, and they are empirically derived [10].

$$K_{SLS,v} = \frac{\rho_m^{1.5} \cdot d}{23}$$
 pre-drilled dowels, bolts, screws, nails, (2.1a)

$$K_{SLS,v} = \frac{\rho_m^{1.5} \cdot d}{30}$$
 nails without pre-drilling. (2.1b)

The German standard DIN 1052 [21] has the same equation but written in terms of characteristic densities instead of mean densities. The Swiss standard SIA 265 [22] also writes $K_{SLS,v}$ in function of characteristic density and the diameter of the fastener in general and only in function of the diameter in the case of nails without predrilling:

$$K_{SLS,v} = 3 \cdot \rho_k^{0.5} \cdot d^{1.7}$$
 general case, (2.2a)

$$K_{SLS,v} = 60 \cdot d^{1.7}$$
 nails without pre-drilling. (2.2b)

The load-to-grain angle is taken into account in SIA 265 by reducing the values by 50% when the load is applied perpendicular to the grain. The current edition of EC5 contains no formula for $K_{SLS,ax}$ of single GiR subjected to tension [20]. Indications on how to compute it in case of GiR inserted parallel

(Equation 2.3) or perpendicular to the grain (Equation 2.4), both expressed as functions of the timber mean density and the rod diameter, were contained in the 2003 draft of EC5 (Annex C of EN 1995-2) [23]. This annexe, however, was omitted from the final published version of the standard [20].

$$K_{SLS,ax\parallel} = 0.04 \cdot d \cdot \rho_m^{1.5}$$
 (2.3)

$$K_{SLS,ax\perp} = 0.08 \cdot d \cdot \rho_m^{1.5} \tag{2.4}$$

Regarding joints that employ laterally-loaded self-tapping screws, the stiffness at SLS $K_{SLS,v}$ is evaluated with the same expressions used for laterally-loaded DTF, i.e. Equation 2.1a. The current edition of EC5 does not specify how to determine the withdrawal stiffness of STS [20].

In the draft for the next generation of EC5 [24], equations are proposed for the axial SLS stiffness $K_{SLS,ax}$ of threaded rods, STS, and glued-in rods (GiR). For threaded rods and STS:

$$K_{SLS,ax} = 160 \cdot \left(\frac{\rho_m}{420}\right)^{0.85} \cdot d^{0.9} \cdot l_w^{0.6}, \qquad \text{Threaded rods, STS} \qquad (2.5a)$$

$$K_{SLS,v} = 60 \cdot d^{1.7}$$
 GiR. (2.5b)

with l_w [mm] denoting the withdrawal length. For laterally-loaded joints realised with GiR or STS, both the current EC5 and SIA 265 apply the same rules of DTF joints (Equation 2.1, Equation 2.2). For joints with inclined STS, the EC5 draft expresses K_{SLS} as a combination of lateral $(K_{SLS,v})$ and axial $(K_{SLS,ax})$ contributions:

$$K_{SLS} = K_{SLS,v} \cdot \sin \gamma \cdot (\sin \gamma - \mu \cos \gamma) + K_{SLS,ax} \cdot \cos \gamma \cdot (\cos \gamma + \mu \sin \gamma) \quad (2.6)$$

 γ is the fastener inclination and μ is the coefficient of friction. The stiffness at ULS is taken as 2/3 of K_{SLS} . This is due to the nonlinear behaviour of timber joints, as the tangential stiffness decreases with increasing load level. However, this is based on old experiments on nailed joints [8]–[10]. The validity of this formula can be questioned for other types of joints or modern applications. According to the current EC5, K_{ULS} should be interpreted as

the secant stiffness between the origin and the design value of the load-carrying capacity.

Ductility

Numerous definitions of ductility exist in the literature. An overview of the different definitions of ductility for joints can be found in [25]–[27].

These definitions are based on displacement or energy, relative or absolute. Displacement-based definitions are written in function of the displacement at the yielding point v_y and also in function of the displacement v_{max} (displacement in correspondence of F_{max}) or the displacement at failure v_u (after F_{max} has been reached). The most common displacement-based definitions of relative ductility are:

$$D_{r,u} = \frac{v_u}{v_u} \tag{2.7}$$

$$D_{r,max} = \frac{v_{max}}{v_y} \tag{2.8}$$

The corresponding absolute definitions are:

$$D_{ab,u} = v_u - v_y \tag{2.9}$$

$$D_{ab,max} = v_{max} - v_y \tag{2.10}$$

Smiths [28] proposed a method for categorising fasteners in timber structures by their ductility ratios. This approach allows joints with comparable load-displacement curves to be grouped. The ductility ratio is computed using both relative and absolute definitions, in line with EC8 guidance [29]. More details about the definitions and the classifications are contained in *Paper I* and in [27].

EC5 states that the load distribution in a structure due to joints of adequate ductility can be considered; however, it does not provide any further explanation or ductility requirements for joints [27]. In the new generation of EC5 [24], an instruction on how to achieve ductile axially loaded GiR joints is given: the yielding of the rods must occur before any brittle failure in the bondline. The following must be satisfied:

$$F_{t,0.95} < F_{w,k} \tag{2.11}$$

where $F_{t,0.95}$ is the 95th-percentile of the resistance of the rod, defined as follows:

$$F_{t,0.95} = A_s \cdot f_{y,0.95} \tag{2.12}$$

 A_s is the nominal stress area for threaded rods or nominal cross-sectional area for ribbed rods, and $f_{y,0.95}$ is the 95th percentile of the capacity of the rod. Another indication is given for joints with laterally-loaded DTF: the joints can be considered "ductile" if two plastic hinges are developed per shear plane. More indications about the term "adequate ductility" can be found in EC8 [29]. Timber structures are classified according to ductility classes.

According to SIA 265 [22], joints with $D_{r,u} = 1$ or 2 (DTF producing < 2 hinges per shear plane) are classified as brittle, whereas those that form at least two plastic hinges per shear plane are classified as ductile ($D_{r,u} \ge 2$).

2.3 Load-displacement curve shapes in timber joint

Analytical expressions for determining the stiffness and load-carrying capacity of joints with DTF utilise key geometrical, mechanical, and loading parameters as input. However, joint behaviour in general is affected by many more factors, not included in the analytical expressions. Moreover, by focusing solely on stiffness, load-carrying capacity, and ductility, one implicitly assumes an elastic-perfectly plastic joint model, even though the actual behaviour might be more complex and nonlinear.

Joints with bolts and dowels

Figure 2.1 shows typical responses for joints with dowels and bolts. Some joints just show the elastic region (curve D1). The joint also shows a plastic region, characterised by a distinct plateau (curve D2), a hardening branch without a clearly defined load-carrying capacity, or a softening branch (curve D4). Some curves can show large plastic displacement and hardening (curve D5). The main geometrical material characteristics of the joints represented

in Figure 2.1 are reported in Table 2.3.

Table 2.3: Characteristics of joint represented in Figure 2.1

Name	Type	Timber	Diameter [mm]
D1 [25]	Multi dowel timber—timber	ST	11.75
D2 [25]	Multi dowel timber-timber	ST	11.75
D3 [30]	Single bolt timber—timber	ST	12
D4 [31]	Single dowel slotted-in plate	GL	16
D5[31]	Single dowel slotted-in plate and reinforcement	GL	16

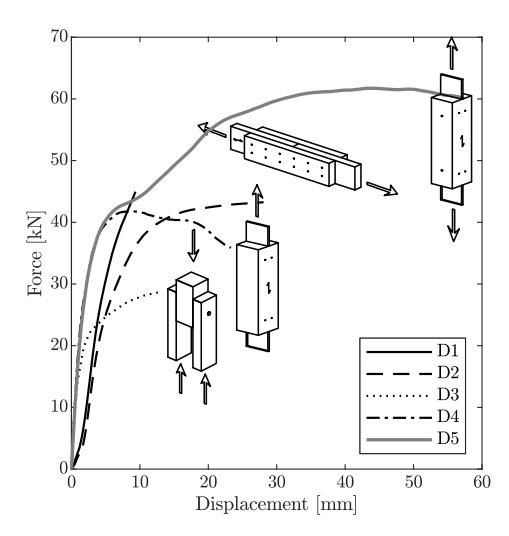


Figure 2.1: Typical load-displacement curves of joints with dowels. Reproduced from the author's own publication: [32] - CC BY 4.0.

Glued-in rods

For joints with GiR whose adhesive bondline fails, the load-displacement curve can be brittle (curve G1 in Figure 2.2) or show a peak followed by softening (curve G2). When the joints are designed to fail in a ductile way, i.e. with the rod yielding, a hardening and ductile response develops (curve G3). Joints

with laterally loaded GiR exhibit a soft and ductile behaviour, similar to that of DTF loaded laterally (curve G4).

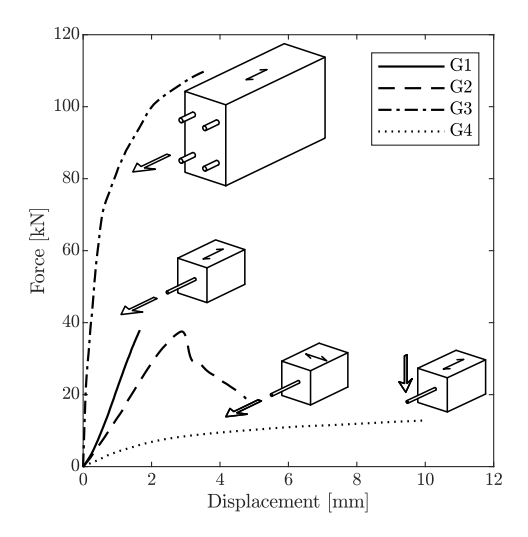


Figure 2.2: Typical load-displacement curves for glued-in-rod joints. Reproduced from the author's own publication: [32] - CC BY 4.0.

Table 2.4: Characteristics of GiR joint represented in Figure 2.2.

Name	GiR	Loading and direction of the load	Timber	Diameter [mm]	Length [mm]
G1 [33]	1	Axial, parallel to grain	LVL	12	150
G2 [33]	1	Axial, perpendicular to grain	ST	12	150
G3 [34]	4	Axial, parallel to grain	ST	20	300
G4 [35]	1	Lateral, parallel to grain	ST	16	320

Self-tapping screws

Axial loading

Several studies investigated the axial (tensile) withdrawal capacity and stiffness of STS in timber. Ringhofer [36] investigated STS in GL and cross-laminated timber (CLT), finding that the wood layup influences withdrawal

performance. STS in CLT (with alternating lamellae) exhibited different with-drawal capacities compared to those in GL. Higher moisture content significantly reduced the withdrawal strength and stiffness, whereas faster loading rates increased the axial capacity. These trends were later confirmed by Toumpanaki [37]. High moisture levels were linked to the screw pull-out failure (withdrawal of the threaded portion) rather than timber splitting, while lower moisture content often led to timber splitting. Brandner [38] investigated the impact of timber species, thread-grain angle, and predrilling on the withdrawal properties of STS. STS in higher-density wood have superior withdrawal strength, e.g. STS in hardwood exhibited greater pull-out capacity than in softwood. This underlined that timber density and layout, e.g. LVL vs solid timber (ST), play a role in the strength of axially loaded STS.

Other researchers focused on the behaviour of a group of STS: Mahlknecht [39] developed a model to predict the block shear failure mechanism for groups of screws in withdrawal. Joyce [40] investigated group effects in axially loaded screws, i.e. how the strength of multiple screws compares to the sum of singles. They found that the number of STS in a joint is did not produce a fully linear capacity increase due to wood failure interactions; however, group action tended to reduce capacity variability (due to homogenization effects and sharing of the loads among the fasteners) and thus to an increase of the 5th-percentile capacity. Moreover, single fastener capacity converged towards the mean value as the size of the STS group increased, so no effective group effect factor at the mean level was found.

Mirdad et al. [41] proposed empirical equations for both the embedment stiffness and withdrawal stiffness of inclined STS, noting that inserting screws at angles (rather than 90°) can markedly increase both capacity and stiffness in joints.

Combined lateral and axial loading

Several studies investigated the behaviour of joints with STS under combined lateral-axial loading [42]–[46]. Blass & Uibel [42] extended Johansen theory to inclined screws by adding the axial component. They also calibrated design parameters by testing by performing embedment and withdrawal tests, and studying spacing/edge-distance limits. Tomasi [43] conducted one of the early comprehensive studies on timber-to-timber joints with laterally and axially loaded inclined screws. The load-to-screw axis, the spacing, and the type

of axial loading (lateral-axial tension and lateral-axial compression loading) were varied. A clear outcome was that the angle of inclination has a large impact on the joint load-displacement curve: smaller angles (more inclined STS) led to significantly higher initial stiffness and higher capacity, but also led to a reduction in ductility. This was also confirmed by an experimental campaign conducted by Jockwer [44], who studied the effects of the load-to-screw axis (angle 45° , 60° , and 90°) under combined shear-tension loading and pulling of the screws. In the test campaign, the behaviour of joints with high-density wood was compared with joints with lower-density wood. The joints characterised by high density exhibited larger stiffness, capacity, and ductility.

Krenn [45] investigated steel-to-timber joints with STS, varying the number of STS in a row, the number of parallel rows, the friction coefficient between steel plate and timber, the friction and the STS angle and performing at least 10 repetitions per configuration. They observed an effective factor on stiffness and capacity of roughly 0.8-0.9 per additional STS, due to wood interactions and system effects. The effect of friction was studied employing a Teflon sheet as an interlayer in one of their series. It was shown how the friction impacted stiffness and capacity. In particular, the lower the friction, the lower the stiffness and the capacity. De Santis [46] investigated the presence of a polyurethane soundproofing layer on the lateral performance of timberto-timber and steel-to-timber joints. Joints with a soundproofing layer showed a large drop in initial stiffness compared to an equivalent joint without the layer, whereas the load-carrying capacity was only moderately decreased (on the order of 10-20%). This effect was more pronounced for configurations with STS at 45° than for those with STS at 90°. Typical curves of joints with STS are illustrated in Figure 2.3. The corresponding characteristics of the joints are reported in Table 2.5.

Table 2.5: Characteristics of STS joint represented in Figure 2.3

Name	Type	Timber	Diameter [mm]	$\overline{\gamma}$
S1 [44]	Timber-to-timber joints	GL	13	90
S2 [44]	Timber-to-timber joints	GL	13	45
S3 [44]	Timber-to-timber joints	GL	13	60
S4 [43]	Timber-to-timber joints	GL	8.2	-45

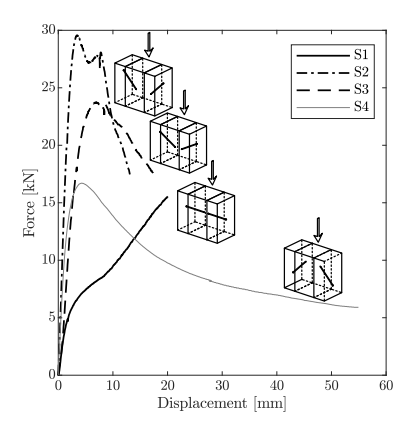


Figure 2.3: Typical load-displacement curves for joints with self-tapping screws. Reproduced from the author's own publication: [32] - CC BY 4.0.

2.4 Modelling of timber joints

To model the load-displacement curve, different approaches can be used. The models can be divided into mathematical, analytical, semi-analytical, and numerical models.

Mathematical models

Mathematical models include rational, exponential, and polynomial functions that were used to model the nonlinear behaviour of timber joints. Some of the models, like the Foschi and Richard-Abbott ones [47], [48], have parameters with a physical interpretation.

In the Foschi model [47] (Equation 2.13), the parameters are the initial stiffness K_{in} , the plastic stiffness K_p and the intercept of the plastic tangent with the vertical axis F_t :

$$F(v) = (F_t + K_p \cdot v)(1 - e^{\left(\frac{-K_{in} \cdot v}{F_t}\right)})$$
 (2.13)

The Richard-Abbott model [48] (Equation 2.14) has an extra parameter:

 a_1 , that shapes the transition between the elastic and plastic ranges. These added parameters make the model less rigid compared to the Foschi one.

$$F(v) = \frac{(K_{in} - K_p) \cdot v}{\left(1 + \left(\frac{(K_{in} - K_p)}{F_r} \cdot v\right)^{a_1}\right)^{\frac{1}{a_1}}\right)} + K_p \cdot v \tag{2.14}$$

Polynomials (Equation 2.15) are continuous and flexible functions. A more complex load-displacement curve can be approximated if a sufficiently high degree of polynomials is selected.

$$F(v) = \sum_{n=1}^{k} p_i \cdot v^i \tag{2.15}$$

Glos and Brandner models describe load-displacement behaviour with rational functions whose coefficients are fixed by boundary conditions [49], [50]. Although these functions offer considerable flexibility, they can become discontinuous where the denominator is zero.

$$F(v) = \frac{v + c_1 \cdot v^{c5}}{c_2 + c_3 \cdot v + c_4 \cdot v^{c5}}$$
 (2.16)

 c_1, c_2, c_3, c_4 are obtained from the curve characteristics by enforcing the following conditions (Equation 2.17-2.20) while c_5 is a shape parameter. Two conditions are imposed on the derivative:

• The initial stiffness is equal to K_{in} (Equation 2.17):

$$\frac{\mathrm{d}F}{\mathrm{d}x}(v=0) = K_{in} \tag{2.17}$$

• The inclination of the curve at the point of the maximum load has to be equal to K_{max} :

$$\frac{\mathrm{d}F}{\mathrm{d}x}(v=v_{max}) = K_{max} \tag{2.18}$$

• The passage of the curve through the point at maximum load F_{max} :

$$\frac{\mathrm{d}F}{\mathrm{d}x}(v=v_{max}) = K_{max} \tag{2.19}$$

• The asymptotic load level F_a that the curve has to approach for large

displacements:

$$F(v \gg v_{max}) = F_a \tag{2.20}$$

Brandner [50] adapts the Glos model by (i) inserting an initial displacement shift v_{in} to capture the initial slip, (ii) adding a linear segment between v_{in} and v_{lin} , and (iii) setting the asymptotic load drop to zero. The expression of the Brander model is:

$$F = \frac{v}{k_1 + k_2 \cdot (v - v_{in}) + k_3 \cdot (v - v_{in})^{k_4}}$$
 (2.21)

with coefficients:

$$k_1 = \frac{1}{K_{in}} (2.22)$$

$$k_{2} = \frac{1}{F_{max} - K_{in} \cdot (v_{lin} - v_{in})} - \frac{k_{4}}{K_{in} \cdot (v_{max} - v_{lin}) \cdot (k_{4} - 1)}$$
(2.23)

$$k_3 = \frac{1}{(k_4 - 1) \cdot K_{in} \cdot (v_u - v_{lin})^{k_4}}$$
 (2.24)

 k_4 governs the curve shape. A comprehensive state-of-art review of other models are available in [32], [51].

Analytical and semi-analytical models

An analytical model refers to a model that provides a closed-form or algebraic solution. In contrast, a semi-analytical model is formulated in closed form but requires an incremental-iterative solution procedure due to the presence of a nonlinear or piecewise constitutive curve for a single-fastener joint, initial slips, or similar complexities. Both analytical and semi-analytical models are developed based on kinematic, equilibrium, and constitutive relationships. These models may also be solved using numerical methods.

Based on some experiments [52], it was observed that in a joint with multifastener (for example, bolts), the load is not shared equally, but typically, the outermost fasteners attract higher forces than those in the middle. This unequal load distribution can lead to premature failures. The concept of a "group action factor" (or effective fastener number) was introduced to account for these effects. In the following years, several studies tried to analytically predict the capacity of a multi-fastener joint to improve design safety ([53]–[56]). Subsequent research advanced the models by incorporating nonlinear curves for fasteners [25], [56], [57]. A more in-depth review of these models can be found in [58].

Analytical models

Lantos model [53], [54]: The goal of the model was to predict the actual force in each of the fasteners of a single-row joint. The model is based on several simplifying assumptions, such as uniform stress in members and a linear load-displacement law for the fasteners.

The joints are a symmetric wood-to-wood splice, composed of two outer members (index O) and an inner middle member (index I). A tensile load P_{max} acts parallel to the grain on a joint of a row of n_f equally-spaced fasteners (spacing equal to S). The model takes the following assumptions:

- Linear-elastic behaviour of the wood and the fastener.
- Constant axial stress across each wood cross-section.
- Identical spacing (S) between fasteners; single fastener row.
- Stiffness of a fastener loaded in shear γ_f (ratio of fastener force to fastener displacement).
- $P_{O,0} = P_{max}$ at one end, $P_{O,n_f} = 0$ at the other.

The interpretation of these parameters is illustrated in Figure 2.4.

 $P_{O,i}$ and $(P_{I,i})$ are the axial force in the outer (inner) member just after fastener i, and Δ_i is the displacement of fastener i.

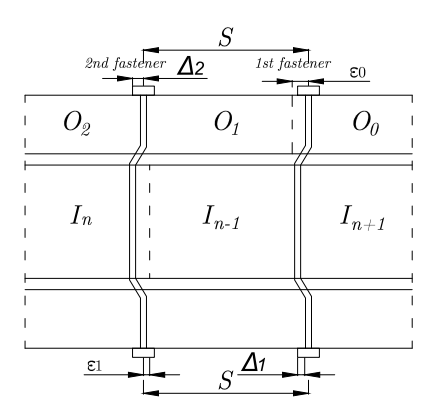


Figure 2.4: Definitions for Lantos model. Redrawn from [53].

Fastener equilibrium:
$$P_{F,i} = P_{O,i-1} - P_{O,i} \ = \ \gamma_f \cdot \Delta_i, \eqno(2.25)$$

Axial strain compatibility:
$$\Delta_i - \Delta_{i+1} = \varepsilon_I S - \varepsilon_O S$$
 (2.26)

$$\varepsilon_O = \frac{P_{O,i}}{E_O \cdot A_O}, \quad \varepsilon_I = \frac{P_{I,i-1}}{E_I \cdot A_I},$$
(2.27)

Cut equilibrium:
$$P_{O,i} + P_{I,i} = P_{max}, \quad i = 0, ..., n_f.$$
 (2.28)

Dimensionless parameters:

$$\omega = 2 + \gamma_f \cdot S \cdot \left(\frac{1}{E_O \cdot A_O} + \frac{1}{E_I \cdot A_I} \right), \qquad \Phi = \frac{\gamma_f \cdot S}{E_I \cdot A_I}. \tag{2.29}$$

Eliminating Δ_i and $P_{I,i}$ from Equation 2.25–Equation 2.28 yields

$$P_{O,i+1} - \omega \cdot P_{O,i} + P_{O,i-1} = \Phi \cdot P_{max}, \qquad i = 1, \dots, n_f - 1.$$
 (2.30)

The characteristic equation of the homogeneous part of Equation 2.30 gives

the roots

$$m_{1,2} = \frac{\omega \pm \sqrt{\omega^2 - 4}}{2}$$
, and define $\mu = \frac{\Phi}{2 - \omega}$.

The general solution is

$$P_{O,i} = A_1 \cdot m_1^x + A_2 \cdot m_2^x - \mu \cdot P_{max}$$

where constants A_1 and A_2 follow from the two boundary conditions $P_{O,0} = P_{max}$ and $P_{O,n_f} = 0$. After substitution, one obtains the closed form

$$P_{O,i} = P_{max} \left[-\mu + m_1^x \cdot (1+\mu) - (m_1^x + m_2^x) \cdot \frac{m_1^x \cdot (1+\mu) - \mu}{(m_2^{n_f} - m_1^{n_f})} \right]. \quad (2.31)$$

The dimensionless factor of "group efficiency" α_{group} can be defined as:

$$\alpha_{group} = \frac{1}{n_f \cdot max(C_1, C_2)} \tag{2.32}$$

Where C_1, C_2 are modification factors. $\alpha_{group} = 1$ would mean perfect, uniform load sharing; typical values are well below 1. The load distribution on the individual fasteners is more uneven when the joined parts are more flexible rather than stiffer, when all other parameters are kept constant. Beyond a certain value of fasteners (n_{max}) , given that the other parameters are fixed, adding more fasteners doesn't increase the total capacity of the connection because the load concentrates near the loaded end.

Equation 2.30-Equation 2.32 therefore provide a complete, force-based prediction of load distribution for any straight row of DTF. The American wood design standards eventually adopted Lantos solution (in a form consolidated by Zahn [59]) to calculate the required group action factor C_q .

Cramer model Cramer [55]: Publishing almost simultaneously with Lantos, [55] presented a combined theoretical and experimental study on the load distribution in steel-to-timber joints with a single row of bolts. All derivations apply only to forces below the proportional limit of wood and steel.

- n_f bolts are arranged consecutively with a constant spacing r.
- Each bolt deforms by a combined slip $y = y_e + y_b$, where

- $-y_e$ is the elastic embedding slip in the wood.
- $-y_b$ is the local bearing-compression of the bolt against the steel plate.
- Axial elongations of the wood core and of the two outer steel plates between two bolts are treated as additional springs in series.
- Stress concentrations around the holes are included with Schulz magnification factor $\beta_{(p),w}$.

The elastic slip in the wood of the bols is:

$$y_e = \frac{\lambda}{k} \frac{\cosh(\lambda \cdot t_w) + \cos(\lambda \cdot t_w)}{\sinh(\lambda \cdot t_w) + \sin(\lambda \cdot t_w)}, \qquad \lambda = \sqrt{\frac{4E_b \cdot I_b}{k_f}}$$
 (2.33)

With E_b and I_b , the bolt Elastic modulus and second moment of area, t_w is the thickness of the wooden member, and k_f is the foundation modulus of the wood.

The local bearing-compression in the steel plates is:

$$y_b = \frac{1}{2t_b \cdot E_b} + \frac{1}{2t_p \cdot E_p}, \tag{2.34}$$

where t_p and E_p are the thickness and elastic modulus of the steel plate.

Taking the reciprocal of Cramer's compliance coefficients gives two dimensionless axial stiffness factors:

$$S_p = \frac{1}{K_p} = \frac{2b_p \cdot t_p \cdot E_p \cdot y}{\beta_p \cdot r}, \qquad S_w = \frac{1}{K_w} = \frac{b_w \cdot t_w \cdot E_w \cdot y}{\beta_w \cdot r}, \quad (2.35)$$

for the steel plates (p) and the wood core (w), respectively. Their ratio

$$\psi = \frac{S_p}{S_w}$$

controls how the external load is shared among the bolts.

The determining equation for the force in fastener i is the following:

$$P_i = P_{i-1} + (K_p + K_w) \sum_{j=1}^{i-1} P_j - K_w F, \qquad i = 2, \dots, n,$$
 (3-73)

with

$$K_p = \frac{\beta_p r}{2 b_p t_p E_p y}, \qquad K_w = \frac{\beta_w r}{b_w t_w E_w y}.$$
 (3-73.a,b)

Where:

 P_i force in fastener i

F external (total) load on the joint

 $\beta_{p(w)}$ Schulz magnification factor for the connected members

 $b_{p(w)}$ width of the connected members

 $t_{p(w)}$ thickness of the connected members

 $E_{p(w)}$ Elastic modulus of the connected members

r fastener spacing

y effective lever arm of the load path

With (p...plate, w...wood). Cramer graphed the percentage load P_i/F for a range of ψ and n_f . For a four-bolt row with identical geometry and the extreme case $\psi = 0.5$, the two outer bolts each carry $P_1 = P_4 \approx 0.33 \, F$, in agreement with Lantos calculation. Once the factor ψ is known, the load of the outer and inner bolt can be determined for any value of n_f .

According to the Cramer model, the load sharing among the bolts depends on the relative stiffness of the steel plate and the wood. The more the timber member and steel plate(s) have comparable stiffness, the more evenly the load is distributed. The opposite happens if one of the two is much stiffer than the other.

Semi-analytical models

Wilkinson [57]: Wilkinson found that Lantos and Cramer ideal elastic models both slightly over-predict the load-carrying capacity of multi-bolt joints due to the nonlinear behaviour of the fasteners. By incorporating piecewise-linear load-displacement curves into the analysis, Wilkinson was able to predict the capacity of multi-fastener joints more accurately.

Wilkinson [57] generalised the analytic approaches of Lantos [53] and Cramer [55] by (i) allowing arbitrary bolt spacing, (ii) incorporating initial slip, and

(iii) assigning an individual, piece-wise linear load-displacement curve to every fastener. The description of the joints is illustrated in Figure 2.5 For bolt

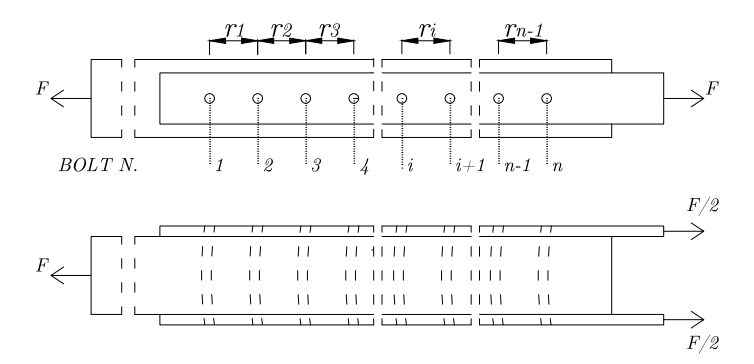


Figure 2.5: Joints analyzed by Wilkinson. Redrawn and adapted from [57].

i on branch j of its experimental load-displacement curve the instantaneous relation is idealised as:

$$\delta_i = \delta_{ji}^* + (P_i - P_{ji}^*) \cdot Y_{ji},$$
 (2.36)

where (δ^*, P^*) denote the end-points of branch j and Y_{ji} is the compliance:

$$Y_{ji} = \frac{\delta_{j(i+1)}^* - \delta_{ji}^*}{P_{j(i+1)}^* - P_{ji}^*}$$
(2.37)

The deformations of the joint components are:

$$r_i + \Delta r_{wi} + \delta_{i+1} = r_i + \Delta r_{vi} + \delta_i \tag{2.38}$$

Where Δr_{pi} and Δr_{pi} are defined as:

$$\Delta r_{wi} = \frac{r_i}{A_w \cdot E_w} \cdot (F - \sum_{k=1}^i P_k) \tag{2.39}$$

$$\Delta r_{pi} = \frac{r_i}{2A_p \cdot E_p} \cdot \sum_{k=1}^{i} P_k \tag{2.40}$$

with spacing r_i , wood area A_w , elastic wood modulus E_w and steel plate

area A_p and elastic steel modulus E_p . Substituting Equation 2.36, Equation 2.39 and Equation 2.40 in Equation 2.38 for the two adjacent segments, $i-1 \rightarrow i$ and $i \rightarrow i+1$, the following Equation can be obtained:

$$\begin{split} -\frac{r_{i-1}}{r_{i}}\cdot Y_{j(i+1)}\cdot P_{i+1} + \left[Y_{ji}\cdot \left(1+\frac{r_{i-1}}{r_{i}}\right) + \frac{r_{i-1}}{2A_{p}\cdot E_{p}} + \frac{r_{i-1}}{A_{w}\cdot E_{w}}\right]\cdot P_{i} - Y_{j(i-1)}\cdot P_{i-1} + \\ \delta_{ji}^{*}\cdot \left(1+\frac{r_{i-1}}{r_{i}}\right) - \delta_{j(i-1)}^{*} - \frac{r_{i-1}}{r_{i}}\cdot \delta_{(j+1)i}^{*} - P_{ji}^{*}\cdot Y_{ji}\cdot \left(1+\frac{r_{i-1}}{r_{i}}\right) + \\ P_{j(i-1)}^{*}\cdot Y_{j(i-1)} + \frac{r_{i-1}}{r_{i}}\cdot P_{j(i+1)}^{*}\cdot Y_{j(i+1)} = 0. \quad (2.41) \end{split}$$

The Equation 2.41 can be written for every bolt of the joint, forming an $n \times n$ linear system that is re-solved at each load increment and the δ^*, P^* terms update whenever a bolt changes branch.

Jorissen: Jorissen [25] improves the Wilkinson and Cramer models by assigning each bolt a nonlinear load-displacement curve, with an initial slip. He also represents the timber between bolts as two parallel springs. The resulting equilibrium-compatibility equations are then solved numerically via an iterative algorithm to calculate the load carried by each bolt. The model assumptions are the following:

- Timber members are symmetric and loaded in pure tension parallel to the grain.
- The wood between adjacent fasteners is linear-elastic; its axial stiffness is represented as follows:

$$k_{s,i} = \frac{E_{s,i} \cdot A_s}{a_{1,i}}, \quad k_{m,i} = \frac{E_{m,i} \cdot A_m}{a_{1,i}}$$

where $a_{1,i}$ is the bolt spacing, E_m and E_s are the Elastic Modulus of the timber of the central and side wood pieces, A_m and A_s are their loaded areas.

• Each dowel is a nonlinear spring with initial slip $\delta_{0,i}$, modelled with the Foschi model:

$$F_i(\delta_i) = \left[F_t + K_{in} \cdot (\delta_i - \delta_{0,i}) \right] \cdot \left[1 - \exp\left(-\frac{K_p(\delta_i - \delta_{0,i})}{F_t} \right) \right], \quad 0 \le F_i \le F_{single}.$$

• Geometric nonlinearities are neglected.

The governing equations are the following:

$$\Delta_{i} = \Delta_{i-1} + \sum_{k=1}^{i-1} \frac{F_{k}}{k_{m,i-1}}$$

$$= \delta_{i} + \sum_{j=2}^{i} \left(\sum_{k=j}^{n_{f}} \frac{F_{k}}{k_{s,j-1}} \right)$$
(2.42)

$$\delta_i = \frac{F_i}{k_{b,i}} \tag{2.42}$$

$$k_{s,i} = \frac{E_{s,i} A_s}{a_{1,i}} \tag{2.42a}$$

$$k_{m,i} = \frac{E_{m,i} A_m}{a_{1,i}} \tag{2.42b}$$

Iterative solution of Equation 2.42 yields the full load-sharing history F_i for n_f fasteners, accounting for progressive engagements of fasteners due to $\delta_{0,i}$.

Adopted semi-analytical joint model: In [56], [60], [61] a semi-analytical joint model based on kinematic and equilibrium considerations was applied to derive the load-displacement and the moment-rotation behaviour of timber joints. The model is based on the following assumptions:

- The deformation of the timber matrix between dowels was neglected.
- Nonlinear springs representing the dowels.
- The fasteners are subjected to the same displacement.

For each displacement increment $\Delta_{\mathbf{v},\mathbf{i}}$, the force in the multi-fastener $\mathbf{F}_{\mathbf{multi}}$ is determined based on the stiffness matrix at that displacement value:

$$\mathbf{F_{multi}} = \mathbf{K} \cdot \Delta_{\mathbf{v}, \mathbf{i}} = \begin{bmatrix} F_{multi, x} \\ F_{multi, z} \\ M_{multi, y} \end{bmatrix} = \mathbf{K} \cdot \begin{bmatrix} \Delta v_x \\ \Delta v_z \\ \Delta \varphi_y \end{bmatrix}, \tag{2.43}$$

With

$$\mathbf{K} = \begin{bmatrix} K_{xx} & K_{xz} & K_{xy} \\ K_{zx} & K_{zz} & K_{zy} \\ K_{yx} & K_{yz} & K_{yy} \end{bmatrix},$$
(2.44)

which contains the axial, the shear and the bending stiffness.

3D and 2D FEM models

An overview of the possible 3D and 2D finite element models is given in [62]. The 3D models can be solid or based on a beam-on-foundation model. The 3D solid FEM models the contact between the fastener and the wood through a surface-to-surface contact with a penalty. Large deformations and convergence problems limit the model applicability. In beam-on-foundations models, the fastener is modelled by a solid element and nonlinear springs are used to model the contact with the surrounding wood [63]. In case of inclined STS, the springs can be placed parallel and perpendicular to the grain direction or placed parallel and perpendicular to the fastener axis. In the first case, they represent the embedment properties parallel or perpendicular to the grain; in the second case, they represent the withdrawal and the embedment properties at an angle to the grain.

2.5 Statically indeterminate structures

This section provides an overview of indeterminate timber structures. Some of the common joint types are described and illustrated through relevant example cases. Structural indeterminacy in timber offers significant potential due to the economy and improved safety through redundancy and load redistribution. It also introduces challenges in analysis, detailing, and construction. Despite these challenges, engineers are drawn to this design approach because it can deliver cost-effective solutions while enhancing structural reliability [64].

Portal frames

Portal frames are usually used in large-span industrial buildings due to their structural efficiency [65]. The joints between the rafters and columns, as well as at the rafter apex, are typically designed as moment-resisting joints (MRJs)

to ensure frame rigidity and lateral stability. The joints can be realised in different ways. Examples of employed joints include joints with dowels and slotted-in plates, which are considered semi-rigid, and GiR or finger joints, which is regarded as clamped [66]. In the case of joints with dowels, different load orientations can be present in multi-dowel joints, which consequently leads to an unequal distribution of the load to the individual dowels. The frame corner can also be realised using GiR or together with steel profiles [67]. Alternatively, also with finger joints can be realized, which are not ductile and are challenging to manufacture onsite. STS are also employed, either to reinforce bolted joints as reinforcement or as the primary fastener in moment joints. An example is the project designed by Woodplan GmbH, which was realised in Risskov, Denmark. The project was an extension to an already existing nursing home, which was built in 2013. The project extends over one plan and will be used as a meeting room for the nursing home's residents. The main structure of the extension is statically independent of the existing building. The project involved steel-to-timber joints with STS. The screws had a nominal diameter of 9 mm and a total length of 380 mm with a load-to-screw axis angle of 45°. This type of joint is illustrated in Figure 2.6.

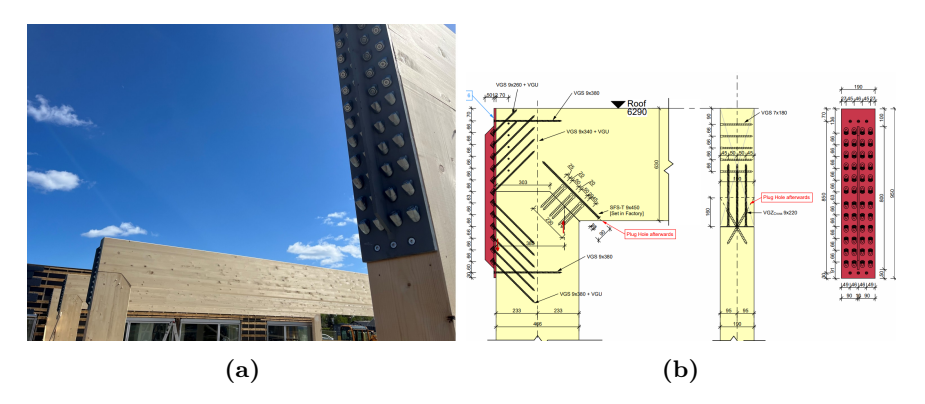


Figure 2.6: Joint in a portal frame with inclined self-tapping screws, Risskov, Denmark. (a) Photo: Woodconstruction A/S, (b) Drawing: Woodplan GmbH.

Continuous floors

Timber concrete composite (TCC) floors are often designed as simply supported. Concrete is used in the compression zone of the floor cross-section, while timber is positioned in the tension zone. These two materials are connected through shear connectors, forming an efficient hybrid system. Projects where TCC floors were employed are e.g. the Anna Freud "Kantor" Centre in London and the eight-storey Life-Cycle-Tower ONE in Austria [68], [69]. TCC floors are primarily used for spans of approximately 6 to 8 m, with their design being predominantly governed by serviceability criteria, such as limiting mid-span vertical deflection. To reduce midspan deflections, multi-span systems might be used. Lately, researchers recognised the potential of multi-span TCC floors and investigated the mechanical behaviour of such floors experimentally and numerically [69], [70]. Continuity transforms a TCC floor from an isostatic, single-span beam into a statically indeterminate plate/beam system that develops both positive and negative bending moments.

Arches and trusses

Traditional arches and trusses are often determinate (e.g. a three-hinged arch, or a simple truss with pinned joints). But variations exist that make them indeterminate; for example, a two-hinged glulam arch (fixed at the base with no hinge at the crown) introduces one extra reaction (horizontal thrust is not statically determinate) [12] (Figure 2.7).



Figure 2.7: Structural systems for arches: three-hinged arch, three-hinged arch with interior joints, two-hinged arch and interior joints.

Modern long-span timber arches (for stadium roofs, etc.) frequently use moment-resisting base connections or splices, making them indeterminate and stiffer. One example of MRj used to splice a three-hinge arch is represented by the Singapore roof structures [11] (Figure 2.8-Figure 2.9). The joint is realised using steel plates and inclined STS, which resist both tensile and compressive

forces generated by moments. Symmetrical central plates on each side resist shear forces.



Figure 2.8: (a) Arch with moment resisting joints during construction, (b) external view of the roof arch. Photo: Ermanno Acler [11].

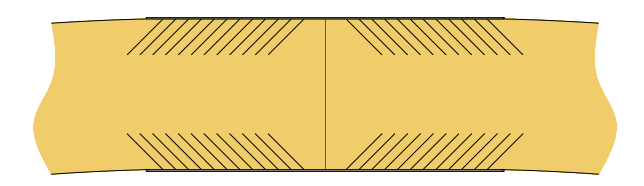


Figure 2.9: Illustration of the moment resisting joints with inclined STS and steel plates used for the arch of the University Sport Hall (Singapore). Reproduced from the author's licentiate thesis [71].

Gridshells and domes

Due to recent advancements in computational technology, the design of complex timber structures such as domes and gridshells has become more popular [72]. These structures primarily resist loads through axial forces in the members. In geodesic domes, composed of rigid triangular units, the loads are distributed without the need for additional bracing. However, joint behaviour is often simplified in design, assuming pinned or clamped joint behaviour, although it significantly affects structural performance and failure. The dominating failure in these structures is usually buckling, which is affected by

the boundary conditions of the members, i.e. by joint stiffness. Similarly, assumptions of joint stiffness are also critical in gridshell for the same motivation. Examples include a reticular dome in Brindisi, Italy, with steel plate joints designed to resist construction-phase forces. In this case, steel plates and inclined STS are used to realise the joints (Figure 2.10).



Figure 2.10: Reticular dome in Brindisi, Italy. (a) internal view, (b) external view. Rubner. Photo: Oliver Jaist Fotografie

2.6 Reliability analysis

Methods of structural reliability

Structural reliability analysis aims to determine the probability of failure of a system according to one or more failure modes in the presence of different uncertainties. Each one of the failure modes is defined by a model and a limit-state function $g(\mathbf{X})$ (also called performance function), and it is expressed as the difference between resistance, R, and load, E. Both capacity and demand depend on the vector of random variables \mathbf{X} .

The probability of failure is defined as follows [73]:

$$P_f = \int_{D_f} f_{\mathbf{X}}(\mathbf{x}) d\mathbf{x} = \int_{\mathbb{R}^n} \mathbf{1}_{D_f}(\mathbf{x}) f_{\mathbf{X}}(\mathbf{x}) d\mathbf{x}$$
 (2.45)

The indicator function $\mathbf{1}_{D_f}(\mathbf{x})$ takes the value 1 in the failure domain D_f and 0 everywhere else:

$$\mathbf{1}_{D_f}(\mathbf{x}) = \begin{cases} 1, & g(\mathbf{x}) \le 0 \\ 0, & g(\mathbf{x}) > 0 \end{cases}$$
 (2.46)

 $f_{\mathbf{X}}()$ is the probability density function of the vector of random variables \mathbf{X} and D_f is the failure domain where $g(\mathbf{X}) \leq 0$. The probability of failure can also be represented using a reliability index, which is defined as follows:

$$\beta_{req} = -\phi^{-1}(P_f) \tag{2.47}$$

 ϕ is the standard normal cumulative distribution function. Except for trivial cases, Equation 2.45 rarely has a closed-form solution. Consequently, approximate analytical methods (e.g., First Order Reliability Method/Second Order Reliability Method), simulation techniques (Monte Carlo, Importance or Subset Sampling), or Adaptive Surrogate-Based approaches (polynomial chaos, Gaussian-process/Kriging models) are employed.

Monte Carlo Simulation

Given a sample of size N of the input random vector \mathbf{X} , the unbiased Monte Carlo Simulation (MCS) estimator of the expectation value in Equation 2.45 is given by [73], [74]:

$$\widehat{P}_f = \frac{1}{N} \sum_{i=1}^N \mathbf{1}_{D_f} = (\mathbf{X}_i) = \frac{N_f}{N}$$
(2.48)

 N_f describes the number of samples such that $g(\mathbf{X}) \leq 0$. For large enough N, the central limit theorem guarantees that \widehat{P}_f follows asymptotically a normal distribution:

$$\widehat{P_f} \sim \mathcal{N}(P_f, \, \sigma_{\widehat{P_f}}^2)$$
 (2.49)

With $\sigma_{\widehat{P_f}} = \sqrt{\frac{1-\widehat{P_f}}{N}}$. The coefficient of variance (CoV) can be calculated as:

$$CoV = \sqrt{\frac{1 - P_f}{N \cdot P_f}} \tag{2.50}$$

This means that when estimating small probabilities of failure, the number

of samples increases. Therefore, for applications that require long computation times, the use of alternative methods, such as approximation or metamodelling methods, becomes necessary.

Approximation methods

Importance Sampling (IS) is a combination of First Order Reliability Method (FORM) and MCS. First, the design point by FORM is computed. Then, a shifted multinormal probability density function (PDF) is used, which is centred around the design point. Thanks to this shift, a smaller sample size is necessary compared to a crude MCS.

An alternative method to reduce the sample size needed to estimate the probability of failure is represented by Subset simulation (Subset). This method was introduced by Au and Beck [75] that translated the problem of estimating a certain probability of failure in solving a series of simpler reliability problems with intermediate failure thresholds. Thus, the probability of failure is calculated as [73]:

$$P_f = \mathbb{P}(D_m) = \mathbb{P}\left(\bigcap_{k=1}^m D_k\right) = \mathbb{P}(D_1) \prod_{i=1}^{m-1} \mathbb{P}\left(D_{i+1} \mid D_i\right). \tag{2.51}$$

With the sequence of failure domains $D_1 \supset D_2 \supset \cdots \supset D_m = D_f$ such that $D_f = \bigcap_{k=1}^m D_k$.

Metamodelling methods

When evaluations are demanding in terms of time, surrogate model-based approaches can be used. The limit state equation in this case is replaced by a metamodel such as Polynomial chaos expansion (PCE) or Gaussian process modelling, also known as Kriging. These samples, however, are generally not optimal for estimating the failure probability. Thus, a more sophisticated methodology, known as active learning, can be employed.

- 1. Based on the experimental design, a surrogate model is built.
- 2. The surrogate model and a reliability estimation algorithm is used to estimate P_f .

- 3. The convergence of the algorithm is checked according three criteria: the first group is related to the learning function, the second one is based on the accuracy of estimated failure probability and last one concerns the stability of the failure probability.
- 4. If the convergence is not reached, the experimental design is enriched by a selection of one pair of sample points \mathbf{X}^{enr} , $g(\mathbf{X}^{enr})$ based on the learning function. The learning function gives information about which points are most likely to increase the accuracy of the surrogate, once added to the experimental design (and thus, of the probability of failure).

The flowchart of this method is illustrated in Figure 2.11.

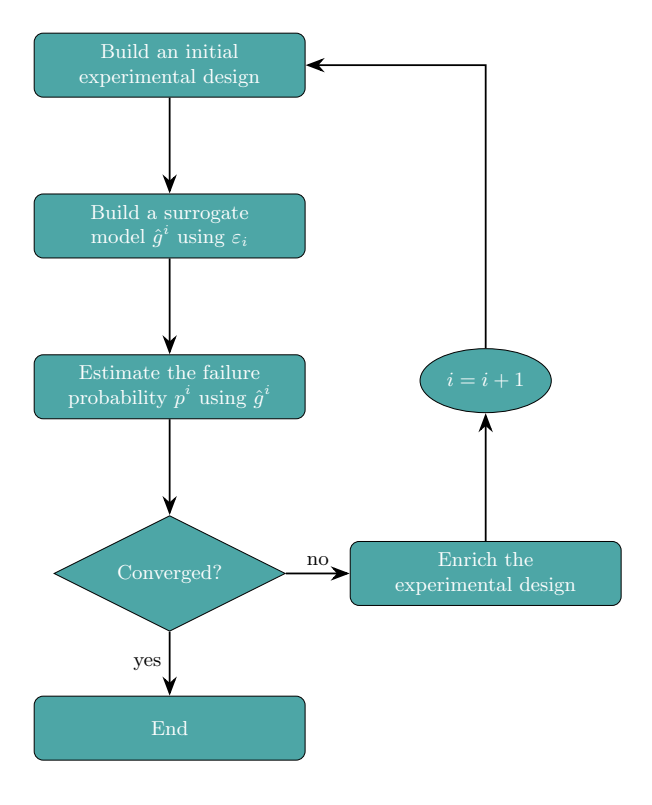


Figure 2.11: Flowchart of the surrogate-model design algorithm.

Reliability of systems

In Section 2.6, methods for estimating Equation 2.45 were discussed. That concerned the component reliability (or failure probability). In reality, structures are more similar to a system made of more than one component. Sudret and Marelli [73] describe a system as "a set of components whose joint functioning is required to ensure the performance of the system." To estimate the reliability of a system, one must identify the configurations of the components within the system.

Three main types of configurations exist:

- 1. Series systems
- 2. Parallel systems
- 3. Mixed systems

The present section focuses on series systems and parallel systems, since the third category can be described as a combination of the first two.

Series systems

A series system appears as a sequence of blocks linked in a line (Figure 2.12).



Figure 2.12: Block diagram representation of a series system

In a series system, the failure of one of the components implies the failure of the whole system. The probability of failure of a series system is the probability of the union of the component failure events:

$$P_{f,series} = \mathbb{P}(\bigcup_{i=1}^{n} F_i)$$
 (2.52)

By De Morgan's law,

$$\mathbb{P}\left(\bigcup_{i=1}^{n} F_i\right) = 1 - \mathbb{P}\left(\bigcap_{i=1}^{n} F_i^{c}\right). \tag{2.53}$$

If the component failures are *independent*, then

$$\mathbb{P}\left(\bigcap_{i=1}^{n} F_i^{c}\right) = \prod_{i=1}^{n} \left(1 - p_i\right) \qquad \Rightarrow \qquad P_{f,series} = 1 - \prod_{i=1}^{n} (1 - p_i). \tag{2.54}$$

For small failure probabilities $(p_i \ll 1)$, only the first-order terms are kept:

$$\prod_{i=1}^{n} (1 - p_i) = 1 - \sum_{i=1}^{n} p_i + \sum_{i < j} p_i p_j - \dots \implies P_{f,series} \approx \sum_{i=1}^{n} p_i, \quad (2.55)$$

neglecting terms of order $p_i p_j$ and higher. The approximation error is $\mathcal{O}(\sum_i p_i^2)$.

Parallel systems

A parallel system is represented by a diagram block with parallel components (Figure 2.13).

$$P_{f,parallel} = \mathbb{P}\left(\bigcap_{i=1}^{n} F_i\right) = \prod_{i=1}^{n} p_i \tag{2.56}$$

In a parallel system, the failure of the system happens only when all the component fails. The probability of failure of such a system is the probability of the intersection of the failure events of each component. In case the failures are independent, then it is equal to the product of each probability.

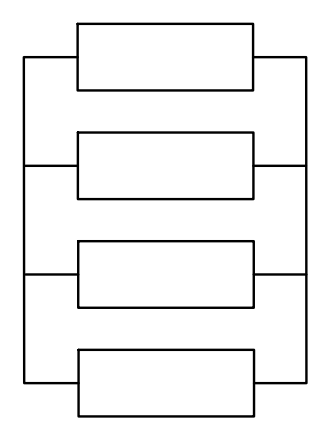


Figure 2.13: Block diagram representation of a parallel system

Reliability studies on timber structures

Several studies investigated the reliability of timber structures regarding the influence of joints [5]–[7], [76]–[78].

Hansson [76] studied the effects of the nonlinear behaviour of nailed joints with punched plates on the reliability analysis of timber trusses. The impact of system effects and the boundary conditions on the reliability of the structure at ULS was studied. Kirkegaard [77] studied how the ductile and timber materials affected the robustness of the timber structures. The outcome was that even a small ductility provides extra reliability. Brühl studied the impact of ductility (and also of the overstrength factor) [78]. It was shown that plastic distribution is possible, provided that joints meet capacity, stiffness and ductility criteria. A reliable overstrength factor was suggested for the case of dowelled joints in a statically indeterminate beam. Schilling [7] investigated the effect of semi-rigid joints on the reliability of timber trusses. While joints are typically assumed to be pinned in trusses, they exhibit nonlinear behaviour in reality. The study revealed that oversimplifying the modelling of these joints results in lower reliability indices, which could lead to potentially unsafe designs. It was shown that modelling these joints simplistically

decreases the reliability indices, leading to potentially unsafe design. Caprio [5] developed a probabilistic model of a statically indeterminate timber beam with joints modelled as elastic, perfectly ductile. The results showed that nonlinear behaviour impacts the reliability of the structure, underscoring the importance of considering nonlinearities in the joints and their related variability.

CHAPTER 3

Analysis

This chapter outlines the methodology used to address RQ1–RQ3. Section 3.1 introduces the case study, which involves the EC5 design of a statically indeterminate timber beam subjected to a uniformly distributed load; this study supports RQ3 and Paper IV. To evaluate system reliability, models for the joints are necessary. Section 3.2 describes the methods for the construction of the empirical-probabilistic model for single-screw joints, addressing RQ1 and references in Paper I and Paper II. Sections 3.3 and 3.4 describe the method for the construction of the semi-analytical model for multi-screw joints. Finally, Section 3.5 formulates the probabilistic model for the case study structure, which is related to RQ3 and is discussed in Paper III and Paper IV.

3.1 The case study

A statically indeterminate beam is the simplest example of a statically indeterminate structure (Figure 3.1). The moments at the joints and midspan moments are written as a function of the coefficients α and β , which depend

on the rotational stiffness of the joints, as follows:

$$\alpha = \frac{K_{\theta, joints} \cdot l}{24 \cdot E_{m, beam} \cdot I_{beam} + 12 \cdot K_{\theta, joints} \cdot l} \quad \text{and} \quad \beta = \frac{1}{8} - \alpha. \quad (3.1)$$

The coefficients α and β describe how the moment at the joint and the midspan change according to the dimensionless stiffness of the joint $k_b = K_{\theta,joints} \cdot l/(E_{m,beam} \cdot I_{beam})$, see Figure 3.2. $K_{\theta,joints}$ is the stiffness of a joint, and $E_{m,beam} \cdot I_{beam}/l$ is the bending stiffness of the beam. On the vertical axis, α and β are plotted in function of k_b .

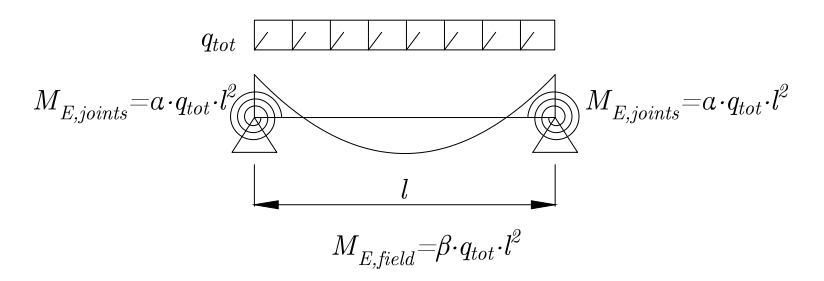


Figure 3.1: Uniformly loaded beam with semi-rigid joints. From Paper IV.

Design of the structure

Different design approaches can be followed for the design of a statically indeterminate beam. For the sake of simplicity, two approaches are selected and discussed: the stiffness-based approach and the capacity-based approach.

The stiffness-based approach follows the following steps:

1. Choice of rigidity level α_{req} :

A rigidity level between 0 and 0.0833 (clamped joint) is selected.

2. Calculation of the maximum moment:

The maximum moment along the beam is calculated as: $M_{E,max} = \max(M_{Ed,joints}, M_{Ed,field})$.

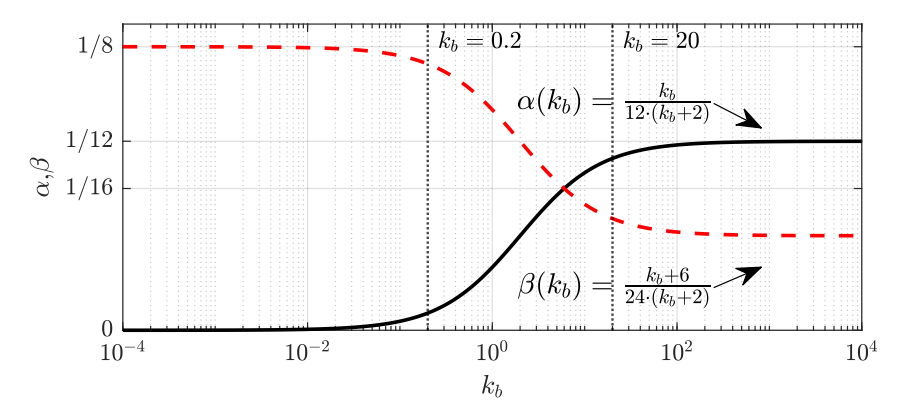


Figure 3.2: Moment at joint and at midspan in function of k_b . Adapted from $Paper\ IV$.

3. Choice of the beam section:

$$h_{beam} = \sqrt{\frac{6 \cdot \max(M_{Ed,joints}, M_{Ed,field})}{b_{beam} f_{m,d}}}$$
(3.2)

4. Selection of n_{screws} :

Assuming the neutral axis is located at the middle of the beam height, the total number of screws on the tension side can be determined as follows:

$$n_{screws} = \frac{K_{\theta,d,ULS,joints}}{K_{\theta,ULS,joints}} = \frac{K_{\theta,d,ULS,joints}}{K_{ULS,joints} \cdot z^2}$$
 (3.3)

 $K_{ULS,joints}$ represents the lateral stiffness at ULS of single-screw joints, while $K_{\theta,ULS,joints}$ is the rotational stiffness of multi-screw joints. The lever arm z, is equal to $h_{beam}/2$. The calculation for $K_{\theta,ULS,joints}$ is as follows:

$$K_{\theta,ULS, joints} = n_{screws} \cdot K_{ULS, joints} \cdot z^2$$
 (3.4)

The capacity-based approach follows Steps 1–3; however, n_{screws} is determined based on the bending capacity of the joints $M_{Rd,joints}$ as n_{screws} =

 $M_{Ed,joints}/M_{Rd,joints}$.

3.2 Model for single-screw joint

Experimental investigation

The experimental program included two phases. An exploratory series and a main test series. An exploratory test series (three replicates per configuration) was carried out to investigate the influence of some of the relevant parameters on the load-displacement curve: test set-up (asymmetric and symmetric), STS length, load-to-screw axis angle, friction, torque, moisture cycling and washer. The load-to-screw axis angle was selected as a parameter to vary in the main test series to study the variability of the load-displacement curve, since varying this parameter markedly changed the shape of the load-displacement curve. In the main test series, the other parameters were kept fixed ($l = 200 \ mm$, $d = 8 \ mm$, $M_{torque} = 15 \ Nm$). Plots of the curves and related discussion on the influence of the parameters can be found in $Paper\ II$. Preliminary report was drafted by undergraduate strudes in a Bachelor thesis supervised by the authour [79].

The main series quantified the variability in the load-displacement curve as a function of the load-to-screw axis angle. All tests used an asymmetric configuration of the test setup. The protocol was based on EN 12512 [80] but displacement-controlled: each specimen was loaded in displacement control at 1mm/min. The loading consisted of a loading up to $40\% \cdot F_{est}$, followed by an unloading phase to $10\% \cdot F_{est}$, and finally a loading phase up to failure. F_{est} is the estimated load-carrying capacity. To eliminate initial slip, a $0.15 \ kN$ pre-tension was applied at the tests of the main test series. Reaction forces were measured by one or two load cells integrated into the test frame.

In the asymmetric setup, a single steel side plate was attached to one side of the timber specimen and subjected to loading. An additional electronic load cell, with a capacity of $220 \ kN$, was connected to the machine load cell to record the applied force (see Figures 3.3a and 3.3b).

The deformations were measured in two ways: digital image correlation (DIC) was mainly used only in the exploratory test series, whereas linear variable displacement transducers (LVDTs) were mainly applied in the main test series. LVDTs were also used for specimens subjected to moisture cycling

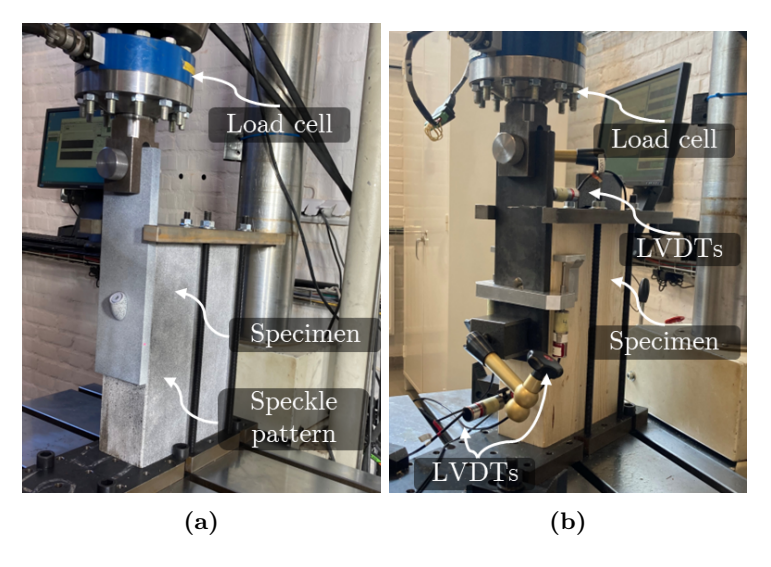


Figure 3.3: The two asymmetric test set-ups used in the experiments. (a): with the DIC system; (b): with LVDTs.

and the joints with rough steel plate surfaces. More details and results about the preliminary test series can be found in $Paper\ II$.

In the main test series, the relative displacement between the steel plate and the timber parallel to the shear plane was measured using LVDTs placed on each side of the joint. Two additional LVDTs were placed at the top and bottom of the steel plate to monitor the movements of the steel plate perpendicular to the shear plane. The displacement was measured relative to the steel plate and in correspondence with the position of the STS (approximately $12 \cdot d$ from the top border of the timber specimen) with a frequency of 8 Hz.

Materials

The steel plates, STS, and washers used in the experiments are shown in Figure 3.4. Three plate variants were employed: (i) a plate with a smooth surface, (ii) a plate that was blast-treated to increase steel-to-timber friction, and (iii) a plate with a smooth surface with two milled holes to evaluate joints with double STS. The blast plate treatment is classified as Sa 2½ (Very Thorough Blast Cleaning) according to ISO 8503 [81]. The washer was only

used in an exploratory test series for joints with a load-to-screw axis angle of 45°. In the main test series, only steel plates with milled holes were used.

The material properties of the STS according to ETA are reported in Table 3.1a. The mean value of the tensile capacity of the screw $(f_{tens,m,exp})$ and the characteristic value of the tensile capacity of the screw $(f_{tens,k,exp})$ were also estimated with experiments, conducting six tensile tests and determining the properties in accordance with ISO 6892 [82]. The experimentally derived properties of the screws are reported in Table 3.1b.

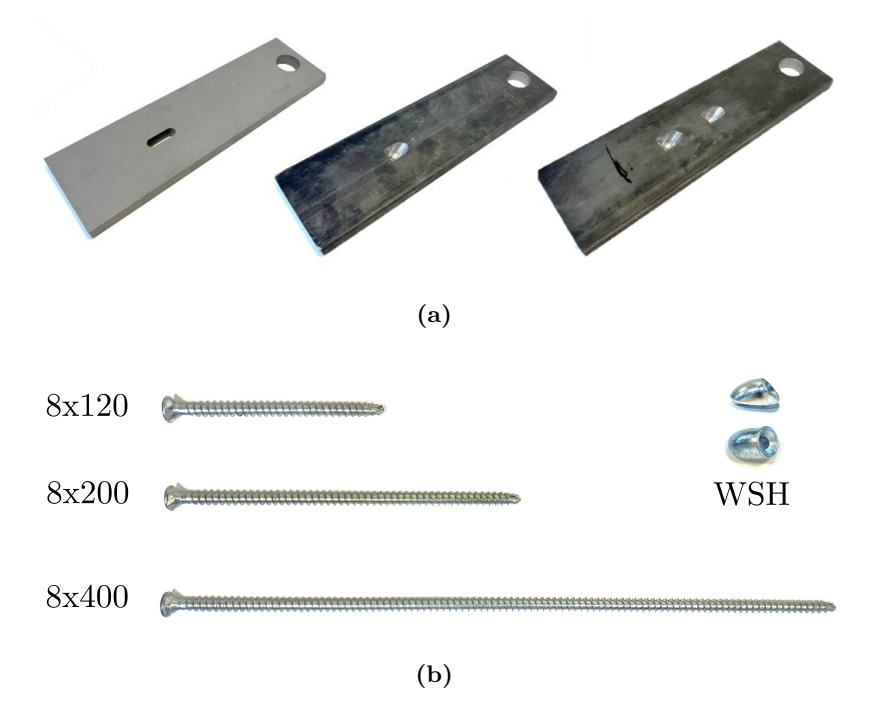


Figure 3.4: (a) Three types of steel plate used, from the left: first is a blast-surfaced plate with an oval hole for the washer, second is a smooth surface plate with a milled hole, and third is a plate with two milled holes for a multi-screw joint. (b) STS of different lengths and washers. Reproduced from the author's own publication: [83] - CC BY 4.0.

Table 3.1: STS geometrical and mechanical properties (a) from ETA-11/0190 [84], (b) from experimental testing.

			(\mathbf{a})			
d [mm]	d_{core} [mm]	l_{screws} [mm]	l_{eff} [mm]	$M_{y,k}$ [Nm]	$M_{tor,k}$ [Nm]	$f_{tens,k}$ [kN]
8	5.1 ± 0.3	120/200/400	97/177/377	23	25	22

	(b))	
$f_{tens,m,exp}$ [kN]	$f_{tens,k,exp}$	[kN]
26.3		23	

Test series and parameters

An overview of the varied parameters with the corresponding number of repetitions is given in Table 3.2. The load-displacement curves of joints with double screw can be found in the Appendix A.

Table 3.2: $l_{screw}=200\ mm$, $d=8\ mm,\ M_{tor}=15\ Nm.$

γ	Repetition	Head tear-off	Withdrawal					
Single-screw joints								
30	10	4	6					
45	20	18	2					
60	10	10	0					
90	20	20	0					
	Double-screw joints							
45	16*	15	1					

Note: (*) 1 repetition presented one STS failing due to tear-off and another screw failing due to withdrawal.

Empirical-probabilistic modelling

Selection of the mathematical model

One of the goals of using parametrised models for the description of the loaddisplacement behaviour of timber joints is to be able to better compare the behaviour of different joint typologies and to assess the variability in the behaviour that is associated with the different parameters. Mathematical models were fitted to the test data, performing regression along a certain region of the curve.

The fitting of the mathematical model to the data was cast as:

$$\min_{P_{mod,1}, P_{mod,2}, \dots, P_{mod,m}} \sum_{j} (f(v_j; P_{mod,1}, P_{mod,2}, \dots, P_{mod,m}) - F_{exp,j})^2, \quad (3.5)$$

where $f(v_j, P_{mod,1}, P_{mod,2}, \ldots, P_{mod,m})$ is the value of the specified regression model that is dependent on the displacement values v_j and on a set of m parameters $P_{mod,1}, P_{mod,2}, \ldots, P_{mod,m}$ (with m depending on the model), and $F_{exp,j}$ is j-th component of the load vector.

The models of Richard-Abbot, Foschi, Brandner, Glos and two polynomials of different degrees were compared in terms of goodness-of-fit and stability. Goodness of fit refers to the ability of a model to reproduce the load-displacement data within the regression interval. Stability refers to the robustness of the fitted parameter set with respect to the intrinsic experimental variability, i.e. the extent to which small perturbations in the data lead to limited changes in parameter estimates of the model.

Determination of the model parameters

After a comparison among different mathematical models, the most suitable one was selected to approximate the nonlinear behaviour of joints with STS; The construction of the empirical probabilistic model of the single-screw joint followed the following steps:

- Step1: Nonlinear regression of the selected mathematical model to the experimental data.
- Step2: Assignment of a probabilistic distribution to each of the model parameters.
- Step3: Determination of the correlation matrix.
- Step4: Generation of synthetic load-displacement curves.

In Step1, a parametrised analytical expression f is used to fit each load-displacement data.

$$y_{\alpha} = f(P_{mod,1,\alpha}, P_{mod,2,\alpha}, P_{mod,3,\alpha}, \dots, P_{mod,m,\alpha})$$
(3.6)

The m parameters of the model are in function of the parameter of influence (in this case, the load-to-screw axis angle).

In Step2 a probabilistic distribution is assigned to each of the parameters, based on empirical fit and theoretical consideration.

$$P_{mod,i} \sim \text{Dist(parameters)}$$
 (3.7)

In Step3, the dependencies among the m parameters and between the parameters and the material properties are taken into account. If the correlation between variables is considered, the parameters should be sampled together from a joint probability distribution of the correlated parameters. This is done by factorising the correlation matrix using the Cholesky decomposition, as follows:

$$\mathbf{C} = \mathbf{L} \, \mathbf{L}^{\mathsf{T}},\tag{3.8}$$

where **L** is triangular (lower or upper). Given a vector of independent standard normal variates yields the correlated random vector **Y**. **X** $\sim \mathcal{N}(\mathbf{0}, \mathbf{I})$, the transformation

$$\mathbf{Y} = \mathbf{L} \mathbf{X} \tag{3.9}$$

C links the material-property vector $\mathbf{M} = (E_{\text{beam}}, f_m)$ with the curve-fit parameter vector of a single-screw joint: $\mathbf{P}_{\text{mod}} = (P_{\text{mod},1}, \dots, P_{\text{mod},m})$.

In MCS every joint is composed of n_{screws} screws, so \mathbf{P}_{mod} was generated n_{screws} times in each run. For every screw $j=1,\ldots,n_{\text{screws}}$ in the joint, and given the material-property realisation $\mathbf{M}=(E_{\text{beam}},\,f_m)$, the associated parameter vector $\mathbf{P}_{\text{mod}}^{(j)}=\left(P_{\text{mod},1}^{(j)},\,\ldots,\,P_{\text{mod},m}^{(j)}\right)$ is sampled conditionally. More details about the procedure are explained in $Paper\ IV$.

In Step4, synthetic data are generated, providing 1, 2, ..., g new load-displacement curves. The number of the sampled curves g is chosen in a way to is statistically representative of the variation of the dataset.

$$y_{1} = f(P_{mod,11,\alpha}, P_{mod,21,\alpha}, P_{mod,31,\alpha}, \dots, P_{mod,i1,\alpha})$$

$$y_{2} = f(P_{mod,12,\alpha}, P_{mod,22,\alpha}, P_{mod,32,\alpha}, \dots, P_{mod,i2,\alpha})$$

$$y_{q} = f(P_{mod,1q,\alpha}, P_{mod,2q,\alpha}, P_{mod,3q,\alpha}, \dots, P_{mod,iq,\alpha})$$
(3.10)

3.3 Model for multi-screw joint

The empirical-probabilistic model of single-screw joint was used as input for the multi-fastener joint model. A different load-displacement curve was STS. The model is based on the following assumptions:

- Timber was assumed to be rigid. Thus, the deformations between the fasteners were neglected.
- Steel plates were assumed to be rigid. Thus, the STS were subjected to the same axial and lateral deformation.
- For each increment in displacement $\Delta_{v,i}$, the force in the multi-screw model could be determined according as:

$$F_{multi,i}(\Delta_{v,i}) = \sum_{j=1}^{n_{screws}} F_{single,j}(\Delta_{v,i}), \qquad (i = 1, \dots, n)$$
(3.11)

Thus, the overall load-displacement curve of multi-screw joints can be obtained.

3.4 Model for moment-rotation curve

The output of the multi-screw joint is then used as input for the moment-rotation model. The rotation point is assumed at the middle of the beam height, and the lever arm is assumed at $z = h_{beam}/2$, the perpendicular distance from the force line of action to the rotation point while $s = h_{beam}$ is the couple arm. Thus, the moment and the corresponding rotation can be writted as:

$$M_{R,joints,i} = F_{multi,i} \cdot s, \quad (3.12)$$
 $\theta_i = \frac{\Delta_{v,i}}{z}, \quad (i = 1, ..., n)$ With n the number of displacement increments.

3.5 Reliability analysis of the structure

In the case of a statically indeterminate timber beam, one performance function is not enough to describe the failure domain of the structure. In fact, the presence of joints introduces additional complexities: failure can occur at midspan, at the joints, or the joints themselves can fail. For each of these cases, a corresponding limit state equation can be defined. The failure at midspan occurs when $g_1 \leq 0$, where g_1 is the following performance function:

$$g_1 = M_{R,beam}(\mathbf{X}) - M_{E,field}(\mathbf{X}) \tag{3.14}$$

The failure at the joints occur when $g_2 \leq 0$, where g_2 is the following performance function:

$$g_2 = M_{R,beam}(\mathbf{X}) - M_{E,joints}(\mathbf{X}) \tag{3.15}$$

 $M_{R,beam}$ is the bending resistance of the beam, $M_{E,joints}$ is the moment acting at joints, $M_{E,field}$ is the moment acting at midspan. Finally, the ultimate rotation at the joints can be exceeded. This turns the system into a simply supported beam, whose failure is defined when $g_3 \leq 0$. g_3 is defined as follows:

$$g_3 = \max(g_{3.1}, g_{3.2}) \tag{3.16}$$

where $g_{3.1}$ is the joints rotation performance function:

$$g_{3.1} = \theta_u(\mathbf{X}) - \theta_{req}(\mathbf{X}) \tag{3.17}$$

 θ_{reg} is defined as:

$$\theta_{req} = \frac{q_{tot} \cdot l^3}{24 \cdot E_{beam} \cdot I_{beam}} - \frac{M_{E,joints} \cdot l}{2 \cdot E_{beam} \cdot I_{beam}}$$
(3.18)

 $g_{3.2}$ is the simply supported beam performance function.

$$g_{3.2} = M_{R,beam}(\mathbf{X}) - M_{max}(\mathbf{X}) \tag{3.19}$$

Since they are independent, meaning that they can be defined mutually exclusive, the total probability of failure is the sum of the single failure probabilities:

$$P_f = P[g_1 \le 0 \ \cup g_2 \le 0 \ \cup g_3 \le 0] \tag{3.20}$$

In some situations, the condition $g_{3.1} \leq 0$ (ultimate rotation of the joints is exceeded) can be considered critical, causing the failure of the entire structure. In this case, $g_3 = g_{3.1}$.

Elastic-perfectly plastic curve

When the joints are modelled with a bilinear curve, the distinction between the elastic and the plastic "mechanism" is possible. In this case, additional limit state equations are needed. This was implemented in *Paper III*, where the distinction was not made in terms of the location of failure, but in terms of brittle/ductile. In particular, three failure modes were identified:

- 1. Brittle/Elastic failure: the resistance was reached at midspan or joints. The equilibrium was reached inside the elastic domain of the joints.
- Ductile/Plastic failure with plastic hinges: the resistance was reached at midspan or joints. The equilibrium was reached inside the ductile domain of the joints.
- 3. Ductile/Plastic failure: the resistance was reached at midspan or joints. The ultimate rotation of the joints was exceeded, and the structural system was evaluated as a simply supported beam.

The probability that "Brittle/Elastic failure" is defined as:

$$P_{b,1} = P[g_1 \le 0 \cup g_2 \le 0 \cap g_{i1} \le 0] \tag{3.21}$$

Where g_{j1} is the performance function that defines the condition of equilibrium reached in the elastic domain of joints, defined as follows:

$$g_{i1}(\mathbf{X}) = M_{E,ioints}(\mathbf{X}) - M_{R,ioints}(\mathbf{X})$$
 (3.22)

Where $M_{R,j}$ is the bending resistance of the joints.

The probability that "Ductile/Plastic failure with plastic hinges" is defined as:

$$P_{b,2} = P[g_1 \le 0 \cup g_2 \le 0 \cap g_{j2} \le 0] \tag{3.23}$$

Where g_{j2} is the performance function that defines the condition of equilibrium reached in the plastic domain of joints, defined as follows:

$$g_{j2}(\mathbf{X}) = M_{E,joints}(\mathbf{X}) - M_{R,joints}(\mathbf{X}) \tag{3.24}$$

Finally, the probability that "Ductile/Plastic failure" occurs after the exceedence of the ultimate joints rotation is defined as follows:

$$P_{b,3} = P[g_2 \le 0 \ \cap g_{i3} \le 0] \tag{3.25}$$

Where g_{j3} is the performance function that defines the condition of exceedence of the ultimate rotation of joints, defined as follows:

$$g_{j3}(\mathbf{X}) = \theta_u(\mathbf{X}) - \theta_{req}(\mathbf{X})$$

Beam-line method

The beam-line method was used to obtain $M_{E,field}$ and $M_{E,joints}$. $M_{E,joints}$ is defined as the intersection between the beam-line and the moment-rotation curve of the joints.

The equation of the beam line is the following:

$$M_{E,joints} = \frac{2}{3} \cdot M_{max} \cdot \left(1 - \frac{\theta}{\theta_{max}}\right) \tag{3.26}$$

 $M_{E,field}$ is obtained as $M_{max} - M_{E,joints}$.

For each load increment j, the intersection between the moment-rotation curve and Equation 3.26 was found. The resulting $M_{E,joints}$ and θ are used to compute the performance functions g_1 , g_2 and g_3 and to verify if any $g_i \leq 0$, indicating failure. More details about the beam-line method can be found in Paper IV.

CHAPTER 4

Results and discussion

This chapter presents the results obtained from the methodology in Chapter 3. First, Section 4.1 reports the EC5 design outcomes for the case-study structure (RQ3). Next, Section 4.2 provides the results for RQ1, namely the empirical-probabilistic model of single-screw joints, as developed in $Paper\ I$ and $Paper\ II$. Section 4.3 then addresses RQ2 by constructing the multi-screw joint model ($Paper\ IV$). Finally, Section 4.4 presents the system reliability analysis for the case study (RQ3; $Paper\ III$, $Paper\ IV$).

4.1 Design of the structure

A joint needs to satisfy both the stiffness and the capacity requirements. For this reason, not all the values of α are feasible. Feasible points first appear at $\alpha \geq 0.077$ for joints with STS inclined 30° or 45° to the load axis, and at $\alpha \geq 0.074$ for joints with a 60° load-to-screw axis angle. All the α values are feasible for joints with a load-to-screw axis angle of 90°. When $\alpha = 0.08$, for joints with load-to-screw axis angle of 90°, a very large number of screws is needed, while for the values $\alpha \leq 0.035$, the design is governed by SLS criteria.

4.2 Single-screw joint model

Selection of the mathematical model

In this section, the models by Foschi, Richard-Abbott, Glos, and Brandner, as well as polynomial models (described in Section 2.4), were applied to a selection of the curves retrieved from the state of the art and the performance of these models is compared. The curves shown in Figure 4.1 were selected to represent a sufficiently diverse range of load-shape behaviours and to test the goodness of the fit of the models.

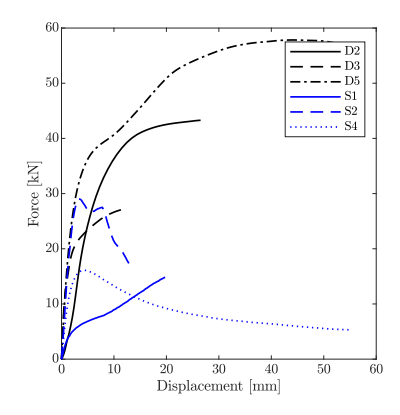


Figure 4.1: Load-displacement shapes considered for the analysis. Reproduced from the author's own publication: [32] - CC BY 4.0.

The performance of the models was evaluated by examining the regression coefficient between the fitted mathematical models and the experimental curve. Among the candidates, the Richard-Abbott model and a 7th degree polynomial demonstrated the best goodness of fit. These two models were subsequently assessed for stability using a dataset of load-displacement curves of timber-to-timber joints with self-tapping screws subjected to combined axial and lateral loading [44]. The parameters of the model in function of the load-to-screw axis angle are illustrated in Figure 4.2. The CoVs for the 7th degree polynomial is generally quite large and often exceeds the changes seen in the parameters associated with variations in density groups or inclinations. This

indicates that the variability in the coefficients is not linked to the variability in the input data; rather, it is associated with the noise in the fitted model. The parameters of the Richard-Abbott model exhibit a clear trend in both the mean value and variability, depending on the load-to-screw axis angle, as well as between datasets characterized by high and low density. The variability of these parameters falls within the expected range for timber joints. Further details regarding parameter estimates can be found in *Paper I*.

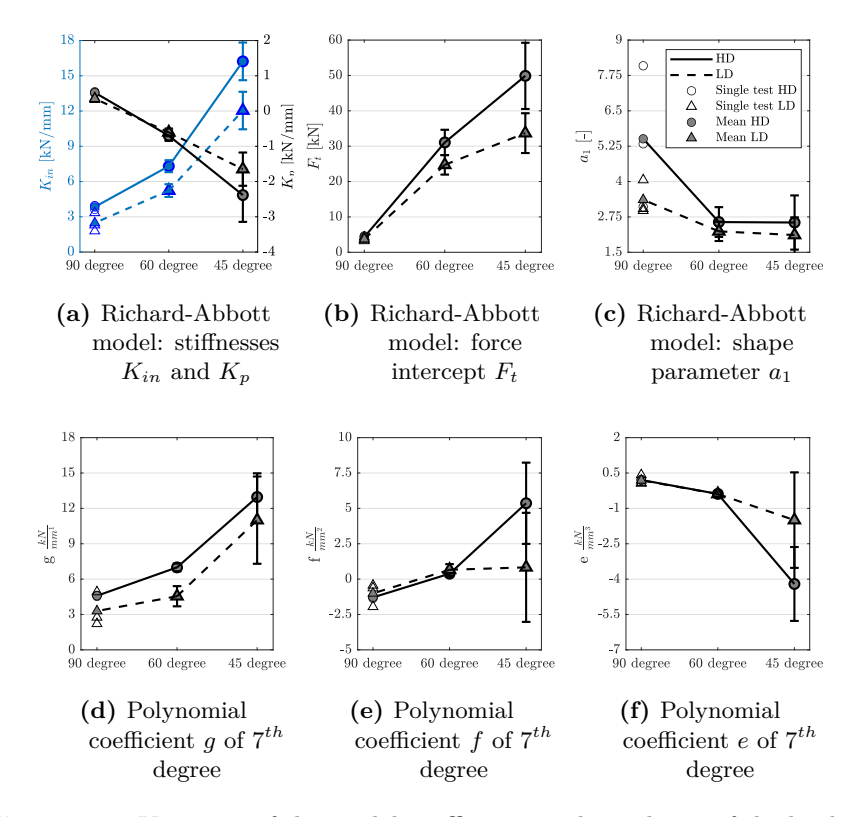


Figure 4.2: Variation of the model coefficients in dependency of the load-to-screw axis angle. Reproduced from the author's own publication: [32] - CC BY 4.0.

Empirical-probabilistic model

Based on the procedure described in Section 3.2, the empirical-probabilistic model of the single-screw joint was developed. The probability distribution of each regression parameter must be identified to accurately model the mechanical behaviour of joints and their variability. Fitting a distribution can also provide insights into the data behavior, variability, and underlying physical phenomena. The distribution is selected based on the variability of the data and the physical meaning of distribution parameters. The values of the parameters K_{in} , F_t , a_1 , and v_u are expected to always be positive; thus, a lognormal distribution is selected for these parameters. A normal distribution is chosen for the parameter K_p since it follows the data and can also assume both negative and positive values. It adapts to the case of joints with inclined STS and softening behaviour (negative value) and to the case of joints with STS perpendicular to the grain with a hardening behaviour (positive value).

An initial slip $v_{in,shift}$, even if this did not occur in the analysed test, might always be possible due to hole tolerance. It is assumed equal to a random realisation from the uniform distribution over the 1 mm hole-clearance tolerance, i.e.

$$v_{in,shift} \sim \mathcal{U}(0, +1 \text{ mm}).$$
 (4.1)

The distribution characteristics for each value of load-to-screw axis angle are summarised in Table 4.1. A probabilistic distribution was assigned to each

Table 4.1: Overview	of the	parameters	and	their	CoV	for	${\it different}$	load-to-
screw ang	les.							

γ	K_{in}	F_t	K_p	a_1	v_u
[°]	[kN/mm]	[kN]	[kN/mm]	[-]	[mm]
30	18.35 (0.21)	$35.1\ (0.06)$	-4.10 (0.14)	8.10 (0.53)	2.53 (0.07)
45	16.24 (0.14)	38.25 (0.24)	-4.90 (0.56)	5(0.31)	2.97(0.13)
60	8.84(0.10)	$39.80 \ (0.25)$	-3.64(0.37)	4.19(0.29)	4.47(0.10)
90	1.63 (0.32)	2.75 (0.75)	0.76(0.20)	7.26 (0.58)	13.85 (0.16)

parameter, and the correlation matrix among the parameters was computed, as illustrated in Table 4.1 and Table 4.2.

For the load-to-screw axis angle of 30° and 45°, both head tear-off failure

	the road to berefit diffe and re-											
γ				30°						45°		_
	F_t	K_p	a_1	v_u	ρ_{den}	E_{beam}, f_m	$* F_t$	K_p	a_1	v_u	ρ_{den}	E_{beam}, f_{m^*}
K_{in}	0.72	-0.72	-0.85	-0.77	0.40	0.20	0.42	-0.49	-0.43	-0.71	0.40	0.20
F_t	1.00	-1.00	-0.60	-0.47	0.40	0.20	1.00	-0.99	-0.81	-0.15	0.20	0.00
K_p		1.00	0.60	0.47	-0.40	-0.20		1.00	0.80	0.19	-0.20	0.00
a_1			1.00	0.46	-0.20	0.00			1.00	-0.07	-0.20	0.00
v_u				1.00	-0.20	0.00				1.00	-0.20	0.00
$ ho_{den}$					1.00	0.60					1.00	0.60
E_{beam}, f_m						1.00						1.00

Table 4.2: Correlation matrix of the regression parameters as a function of the load-to-screw axis angle.

γ				60°						90°		
	F_t	K_p	a_1	v_u	ρ_{den}	E_{beam}, f_m	$*$ $ $ F_t	K_p	a_1	v_u	ρ_{den}	E_{beam}, f_{m^*}
K_{in}	-0.25	0.26	0.14	-0.79	0.40	0.20	0.10	0.28	-0.19	-0.50	-0.40	-0.20
F_t	1.00	-0.95	-0.93	0.60	0.20	0	1.00	-0.75	-0.40	0.10	-0.20	0
K_p		1.00	0.86	-0.48	-0.20	0		1.00	0.40	-0.34	0.00	0
a_1			1.00	-0.51	-0.20	0			1.00	0.02	0.00	0
v_u				1.00	-0.40	-0.40				1.00	0.40	0.20
ρ_{den}					1.00	0.60					1.00	0.60
E_{beam}, f_m						1.00						1.00

^{*} The correlation between E_m and f_m is set to 0.8 as prescribed by JCSS [18].

and withdrawal failure of the STS occurred. The load-displacement curves presented different characteristics: head-tear off failure of the screw resulted in a drop in load at the failure point, while withdrawal failure of the STS resulted in a softening post-peak behaviour. Therefore, the random curves are generated reflecting the probability of occurrence of a failure mode, calculated as:

$$P_{HTO} = \frac{n_{HTO}}{n_{tot}}, \quad P_{WITH} = 1 - P_{HTO}.$$
 (4.2)

 P_{HTO} is the probability of occurrence of the head-tear off failure, P_{WITH} is the occurrence of the withdrawal failure, n_{HTO} is the number of tests characterized by head-tear off failure, while n_{tot} is the total number of the tests. For joints with STS with load-to-screw axis angle of 30°, $P_{HTO} = 60\%$,

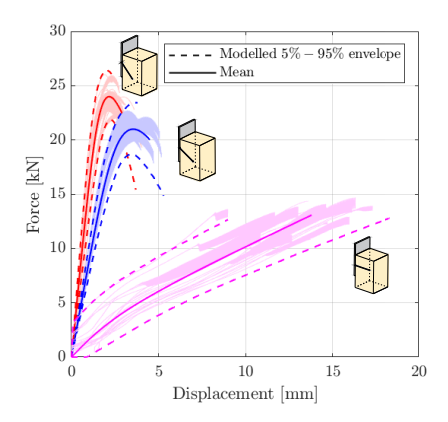


Figure 4.3: Generated load-displacement for load-to-screw axis angles of 90°, 60°, and 45°. Reproduced from the author's own publication: [83] - CC BY 4.0.

 $P_{WITH} = 40\%$. For the angle 45°, $P_{HTO} = 90\%$ and $P_{WITH} = 10\%$. For the angles of 60° and 90°, $P_{HTO} = 100\%$.

Since the variability of the parameters in case of withdrawal failure of the STS cannot be reliably determined, the load-displacement curve and its variability are assumed identical to those of head tear-off, with the sole modification that the curve is extended until the load decreases to zero rather than truncated at the ultimate displacement v_u .

Sampling synthetic curves from the model yields load-displacement curves whose envelope fully contains the experimental load-displacement curves, as can be observed in Figure 4.3.

4.3 Multi-screw joint model

The empirical-probabilistic model for single-screw joint developed in Section 4.2 was used as input for developing a semi-analytical (statistical) model of multi-screw. Three characteristics that usually describe the shape of a load-displacement curve: the mean elastic secant stiffness K_{10-40} , the mean capacity F_{max} and the mean absolute ductility D_{ab} . K_{10-40} was computed as secant stiffness at to load levels (40% F_{max} and 10% F_{max}), The load-carrying

capacity F_{max} is the maximum force the joint can experience, and the ductility follows the absolute definition, i.e. $D_{ab} = v_u - v_y$. v_y is the displacement at the yielding point, and v_u is the ultimate displacement at failure or a 20% drop of the curve after the load peak. Increasing n_{screws} had no effect on K_{10-40}/n_{screws} , F_{max}/n_{screws} and D_{ab} for all the angle except for the 90° case. In this case, F_{max}/n_{screws} and D_{ab} notably decreased. The introduction of initial slip had small effect on K_{10-40}/n_{screws} for all the angles, while no remarkable effect either on F_{max}/n_{screws} and D_{ab} and on relative CoVs compared to the case of no initial slip. As n_{screws} increases, the CoVs for every angle falls with each additional screw. All the discussed effects diminish and eventually plateau: the mean values of K_{10-40}/n_{screws} , F_{max}/n_{screws} and D_{ab} converge, falling to asymptotic levels (Figure 4.4).

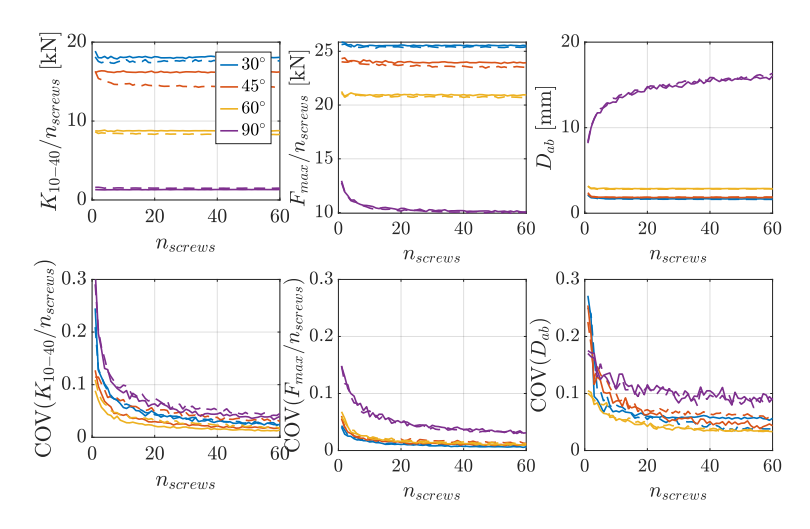


Figure 4.4: Variation of the mean values of $K_{10\text{-}40}/n_{screws}$, F_{max}/n_{screws} , and D_{ab} and related CoVs in function of n_{screws} . From $Paper\ IV$.

4.4 Reliability analysis of the structure

In the first part, different methodologies to estimate the reliability of the structures are compared in terms of computational time and accuracy. In the second part of this subsection, after the selection of the most suitable methodologies, the full reliability analysis is performed on the statically indeterminate timber beam incorporating nonlinear joint behaviour and the related variability.

Methodology selection

MCS, Subset, IS and APCK-Subset were evaluated on the structure in Figure 3.1, assuming an elastic-perfectly plastic material model. The characteristic load was taken as $G_k = 4.6 \ kN/m$, a typical value for roof beams. Timber grade C24 served as the material basis for all calculations. The probabilistic analysis was performed using UQLAB toolbox [74]. The maximum sample size was set as the stopping criterion for MCS, Subset, and IS. MCS was tested setting the maximum sample size equal to 10^7 and 10^6 . The initial value m_0 for the Active learning algorithm was set to 10. The algorithm was stopped when the maximum sample size was reached or the default convergence criteria were met.

The resulting probabilities of failure are summarised in Table 4.4. MCS (maximum sample size equal to 10^6) returned a good estimation of the probability of failure in relatively low computational time. The accuracy can be improved by increasing the sample size, but at the expense of computational time. For example, increasing the sample size from 10^6 to 10^7 resulted in increased computational time by a factor of ≈ 45 .

	1			
Method	Evaluations	P_f	CV	Time
MCS	10^{7}	$2.85 \cdot 10^{-4}$	0.02	89.44 sec
MCS	10^{6}	$2.76 \cdot 10^{-4}$	0.06	$2.18 \sec$
Subset	36998	$2.56 \cdot 10^{-4}$	0.09	$0.17 \sec$
IS	1196	$2.94 \cdot 10^{-4}$	0.07	$0.32~{ m sec}$
APCK-Subset	162	$4.02 \cdot 10^{-4}$	0.02	$1211 \sec$

Table 4.4: Comparisons of different reliability methods.

Subset required a smaller sample size ($\approx 3 \cdot 10^4$), but the estimation is characterised by less accuracy (CoV = 0.09) if compared to MCS. IS requires an even smaller sample size ($\approx 1 \cdot 10^2$), with improved accuracy (CoV = 0.07) if compared to Subset, but less accuracy if compared to MCS with a sample size of 10^7 . APCK-Subset did not return a satisfactory estimation of the

probability of failure due to the complexity of the problem and the larger number of performance functions involved.

Full reliability analysis

A comprehensive reliability analysis was conducted, considering the nonlinear behaviour of the joints. The MCS sample size $(2 \cdot 10^6)$ was calibrated to achieve an accurate estimation of the target failure probability, $P_f = 2.2 \cdot 10^{-5}$. The resulting estimate has a CoV of 0.15. The input variables are listed in Table 4.5.

Table 4.5: Distribution parameters of the considered random variables.

Input variable	Unit	Distribution	Char V.	Mean V.	CV
G^*	$\frac{kN}{m}$	Normal	-	0.65	0.1
Q^*	$\frac{kN}{m}$	Gumbel	5.85	3.21	0.3
f_m^*	$\frac{\overline{m}_{N}}{\overline{m} m^{2}}$ $\frac{N}{m m_{o}^{2}}$	Lognormal	30	38.8	0.15
E_{beam}^*	$\frac{N}{mm^2}$	Lognormal	-	13'000	0.13
W_{el}	m^{-3}	Constant	Design	n based	-
<u>l</u>	m	Constant	-	10	-

^(*) Based on the indication contained in JCSS [18].

First, the influence of the ratio K_{ULS}/K_{SLS} on P_f was studied, then for the case when P_f did not meet the target values, the ratio K_{ULS}/K_{SLS} was calibrated to restore the target value of P_f .

Influence of the ratio K_{ULS}/K_{SLS}

For the case $K_{ULS}/K_{SLS}=2/3$, the failure probability P_f exceeds the target value when $\alpha \leq 0.07$ for joints with a load-to-screw axis angle of 90°. For all other angles, P_f remains close to the target across the examined range of α (Figure 4.5). For the case $K_{ULS}/K_{SLS}=1$, P_f exceeds the target value for joints with a load-to-screw axis angle of 90° and $\alpha \leq 0.07$. For the other angles P_f stays unchanged for the feasible values of α (Figure 4.6).

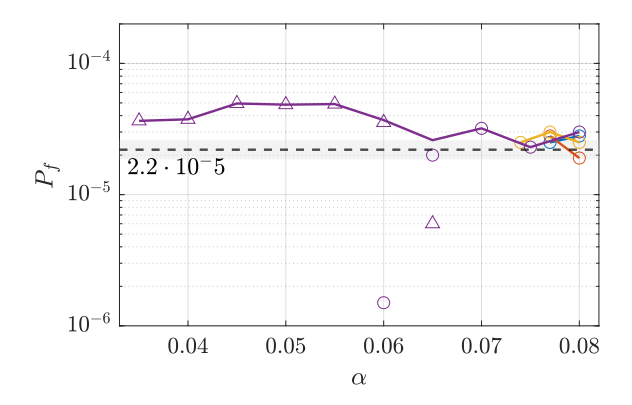


Figure 4.5: Probability of failure as a function of α ($K_{ULS}/K_{SLS}=2/3$). From *Paper IV*.

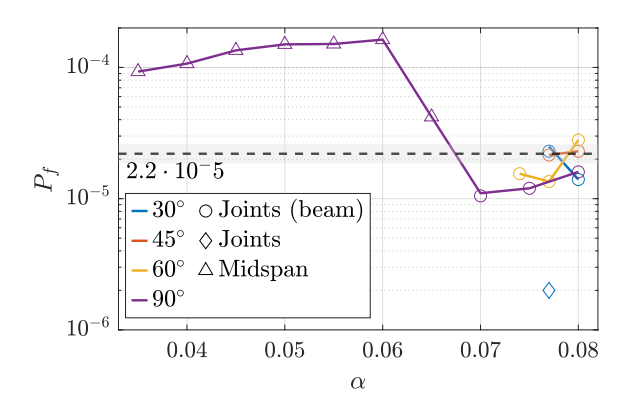


Figure 4.6: Probability of failure as a function of α ($K_{ULS}/K_{SLS}=1$). From *Paper IV*.

Calibration of the ratio K_{ULS}/K_{SLS}

For cases where the estimated failure probability P_f exceeded the target, the ratio K_{ULS}/K_{SLS} was calibrated. A combined grid-search and bisection algorithm was employed to determine the ratio that satisfies the target value of P_f . The calibrated ratio can be written as a function of α . For $\alpha \leq 0.063$,

the ratio is almost constant, with an average value of 0.56. For $\alpha \geq 0.067$, the ratio is constant and equal to 1 (Figure 4.7). This can be explained by the fact that when the joints are designed as clamped or close to clamped conditions, the equilibrium points fall inside the elastic region, making redundant the use of the stiffness reduction ratio. For the other load-to-screw axis angle, no calibration was needed, since P_f already was within a threshold of the target value. In this case, the ratio K_{ULS}/K_{SLS} is equal to 1.

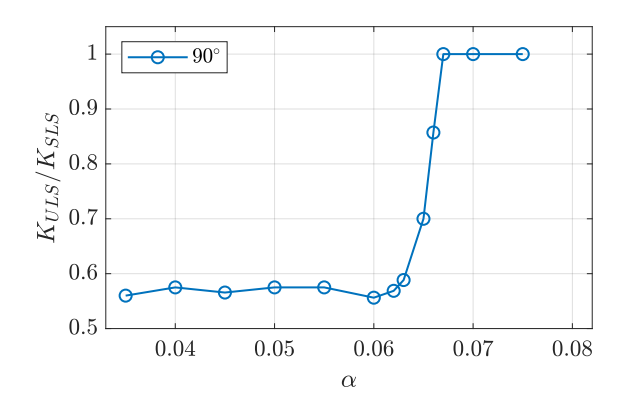


Figure 4.7: Calibration of the ratio K_{ULS}/K_{SLS} in function of α . From *Paper IV*.

CHAPTER 5

Conclusions and future work

5.1 Conclusions

Despite advances in timber design codes, the reliability of statically indeterminate beams with nonlinear joints remains underexplored. This thesis aims to quantify the structural reliability (probability of failure P_f /reliability index β_{rel}) of statically indeterminate timber beams by explicitly modelling the nonlinear behaviour and statistical variability of the joints together with material and load uncertainties. To achieve this aim, a three-level probabilistic framework was developed, from the development of the single-screw model to the development of the probabilistic model of the structure. This chapter presents the main conclusions of this thesis. Following the general conclusions, the main findings are organized in relation to the research questions described in Section 1.2.

General conclusions

The empirical probabilistic model is useful to model the nonlinear behaviour of joints and their variability. It can serve as input for a more complex model involving multiple screws, as well as for structural modelling and reliability analysis. This will allow structural analysis of complex structures at different load levels. The multi-screw joint illustrates how the variability in the load-displacement curve, along with associated properties like stiffness, capacity, and ductility depends on the number of fasteners used.

Results of the calibration of the stiffness reduction ratio highlighted how the stiffness reduction ratio depends on the nonlinear behaviour of the specific joints where the equilibrium points fall inside the joint curve. A unique ratio can hardly cover all the design situations conservatively. The use of calibrated stiffness ratios ensure the target level of reliability.

RQ1: Single-screw joint model

Two inputs were required to answer RQ1: (i) a mathematical model that could approximate the nonlinear load-displacement curve and the related variability; (ii) experimental data as a basis for the single-screw model.

Foschi, Richard-Abbott Glos, Brander, and polynomial models were fitted to representative experimental load-displacement curves of timber joints from the state of the art, and the goodness of fit was evaluated. Subsequently, the stability, i.e. how well the models represent the variability of the curves, of two best models in terms of goodness of fit: the Richard-Abbott model and the polynomial of 7th degree, was evaluated. The main conclusions of the thesis were the following:

• Mathematical model comparision:

The models of Foschi and Richard-Abbott are comparably simple and showed good performance on curves with or without softening. They can be too rigid to represent the local features of some curves, such as hardening or residual capacity at very large displacements. The Brandner and Glos models can approximate the softening with a nonlinear trend. However, they are not suitable to represent the load-displacement curves without softening branches. A Polynomial of sufficiently high degree can approximate curves characterised by very complex shapes, but they fail to represent the variability associated with the load-displacement curve.

• Consideration of the initial slip:

For any model, a small horizontal shift to the load-displacement curve can be applied, representing the initial slip. Alternatively, when using the Glos model or a sufficiently high-degree polynomial, the initial slip is directly formulated in the model, preserving the continuity of the function throughout.

• Mathematical model stability:

Only the Richard-Abbott model was able to capture the variability in the test data through its regression parameters, whereas fitting a polynomial of $7^{\rm th}$ degree to the curves resulted in significant parameter estimates with noise.

An experimental campaign was conducted on steel-to-timber single-screw joints at several load-to-screw axis angles, with 10–20 repetitions per configuration to characterise the variability. Once a suitable mathematical model and the experimental data were obtained, the construction of the empirical-probabilistic model could be initiated. The following conclusions were derived:

• Probabilistic distribution assignment:

A lognormal distribution for the Richard-Abbott parameters K_{in} , F_t , a_1 was acceptable for both the goodness of fit and physical interpretation, since these parameters are always expected to be positive. A normal distribution was better suited for the parameter K_p , since it can assume positive values if the curve is characterised by a hardening trait, or negative values if it is characterised by softening. An additional parameter v_u was introduced to define the value of the displacement at which the curve should be stopped. A lognormal distribution was then assigned to this parameter.

• Validation:

Monte Carlo generated synthetic curves reproduced the experimental load-displacement curves: the 5–95% percentile envelope of the synthetic load-displacement curves fully contained all observed test curves, supporting the model validity.

Forward applicability:

The model can be used as input for a multi-screw model (RQ2) that can consequently be used in structural and reliability analyses (RQ3).

RQ2: Multi-screw joint

Based on RQ1, the single-screw load-displacement curve was used as input to a semi-analytical, displacement-controlled model for multi-screw joints. The trend of the normalised values of stiffness, load-carrying capacity and ductility per STS was studied as a function of the number of STS. The following conclusions were drawn:

• Evolution of mean properties with the number of screws:

For all screw orientations except 90°, the mean values of stiffness, load-carrying capacity normalised per STS, and the mean value of ductility, remain essentially constant as the number of STS increases. For joints with STS inclined at 90° while the stiffness per STS also remains constant, the mean capacity and ductility per STS decrease slightly with increasing STS before levelling off near their asymptotic values.

• Evolution of the variability with the number of screws:

As the number of STS increases, the coefficient of variation in stiffness, capacity, and ductility decreases monotonically, approaching asymptotic values.

Influence of the initial slip:

Incorporating an initial slip randomly assigned between 0 and 1 mm to each load-displacement curve only affects the normalised stiffness per screw: its mean value decreases slightly with increasing number of STS before converging to an asymptotic value, while the other properties and the related CoVs remain unchanged.

RQ3: Reliability of the structure

Three inputs were needed to answer RQ3: (i) an adequate methodology to estimate the probability of failure and a probabilistic model of the structure, (ii) a probabilistic model of the structure, (iii) the multi-screw joint model (developed in RQ1 and RQ2). A preliminary reliability analysis was used to identify the correct methodology to estimate the reliability of statically indeterminate timber structures. Uncertainties were assigned to loads, materials, and nonlinear behaviour of joints. MCS, IS, Subset and APCK-Subset

were compared in terms of accuracy and computational time. Based on this preliminary analysis, the following conclusions were drawn:

• Reference probability of failure:

MCS with 10^7 samples returned $P_f = 2.85 \cdot 10^{-4}$ (CoV = 2 %), adopted as the benchmark for method comparison. Reducing MCS to 10^6 samples changed P_f by only -3.2%, indicating that (10^6) simulations already provide an acceptably stable estimate for that case study.

• Surrogate-based bias:

APCK-Subset delivered a markedly higher $P_f = 4.02 \cdot 10^{-4}$. Thus, the accuracy of reliability methods relying on the reconstruction of the limit state equation, such as APCK-Subset, might be affected by approximation errors as the number of performance functions and failure modes increases.

Performance of other sample size reduction methods:

Subset required only a number of evaluations equal to $\approx 3 \cdot 10^4$, but it decreased accuracy (CoV =0.09). IS required even fewer evaluations ($\approx 1 \cdot 10^3$) with a similar accuracy (CoV=0.07).

• Selection of the method:

Given the accuracy of MCS and possible approximation error using methods that rely on approximation methods and on the reconstruction of the performance function, MCS was selected as a method for the reliability analysis of the statically indeterminate beam.

After the selection of the methodology, the nonlinear behaviour of joints was included in the model (RQ3). The statically indeterminate timber beam was designed according to EC5. The influence of the ratio K_{ULS}/K_{SLS} on the reliability of the structure was studied. The following conclusions were drawn:

Non-uniqueness:

The ratio K_{ULS}/K_{SLS} cannot cover all the design situations and joint typologies.

• Influence of the current prescribed value of 2/3:

The current prescribed ratio $K_{ULS}/K_{SLS} = 2/3$ is overconservative for joints with 30°, 45°, 60°, 90° for joints in the clamped region, since the probability of failure stays the same, but the joints requires a larger number of STS. It is instead unconservative for the case 90°, when the joints are within the semi-rigid region.

• Calibrated values:

For 30°, 45°, 60°, the calibrated stiffness ratio K_{ULS}/K_{SLS} is 1 for all feasible α values (no reduction), because the joints are designed close to clamped and are used in the elastic range. For 90°, the calibrated ratio averages 0.56 when $\alpha \leq 0.070$ and equals 1 for $\alpha > 0.070$.

5.2 Future work

Based on the findings of this thesis, several directions for further research were identified. These are outlined below.

Single-screw joint model extension

The Richard-Abbott model provided a good approximation of the load-displacement curve of the timber joints with STS. However, it could not fully reproduce certain local features of the post-peak softening branch, i.e. the small residual load-carrying capacity that can appear at very large displacements. Because this region contributes little to serviceability or ultimate limit states, the reliability impact was limited; however, achieving a faithful representation at large displacement would improve predictions for design situations involving extreme deformation or progressive damage. Future work could explore hybrid formulations involving multiple mathematical functions.

In the experimental campaign, only the load-to-screw axis angle was varied. Other additional parameters of influence exist, such as timber density, STS diameter, thread geometry, penetration depth, friction, and moisture variation. All these parameters affect the load-displacement curve. Consequently, the validity of the empirical-probabilistic model cannot be assumed outside the range of density and geometry adopted. A larger test database is required to strengthen the validity of the model.

Multi-screw joint model extension

In practice, a joint rarely experiences a single load component; bending moments, shear forces and axial tension or compression typically act simultaneously, so a realistic timber joint model must account for their simultaneous action and interaction.

A future advancement of the model is to introduce dependency on the spacing among the STS. The spacing affects the force in the single-screw joint and consequently, the overall load-displacement curve of the multi-screw joint.

Reliability of the structure

Due to the limited experimental data, the correlations among joint model parameters and between the joint parameter and the material properties of timber should be regarded as approximate. Increasing the number of experiments would reduce the uncertainties.

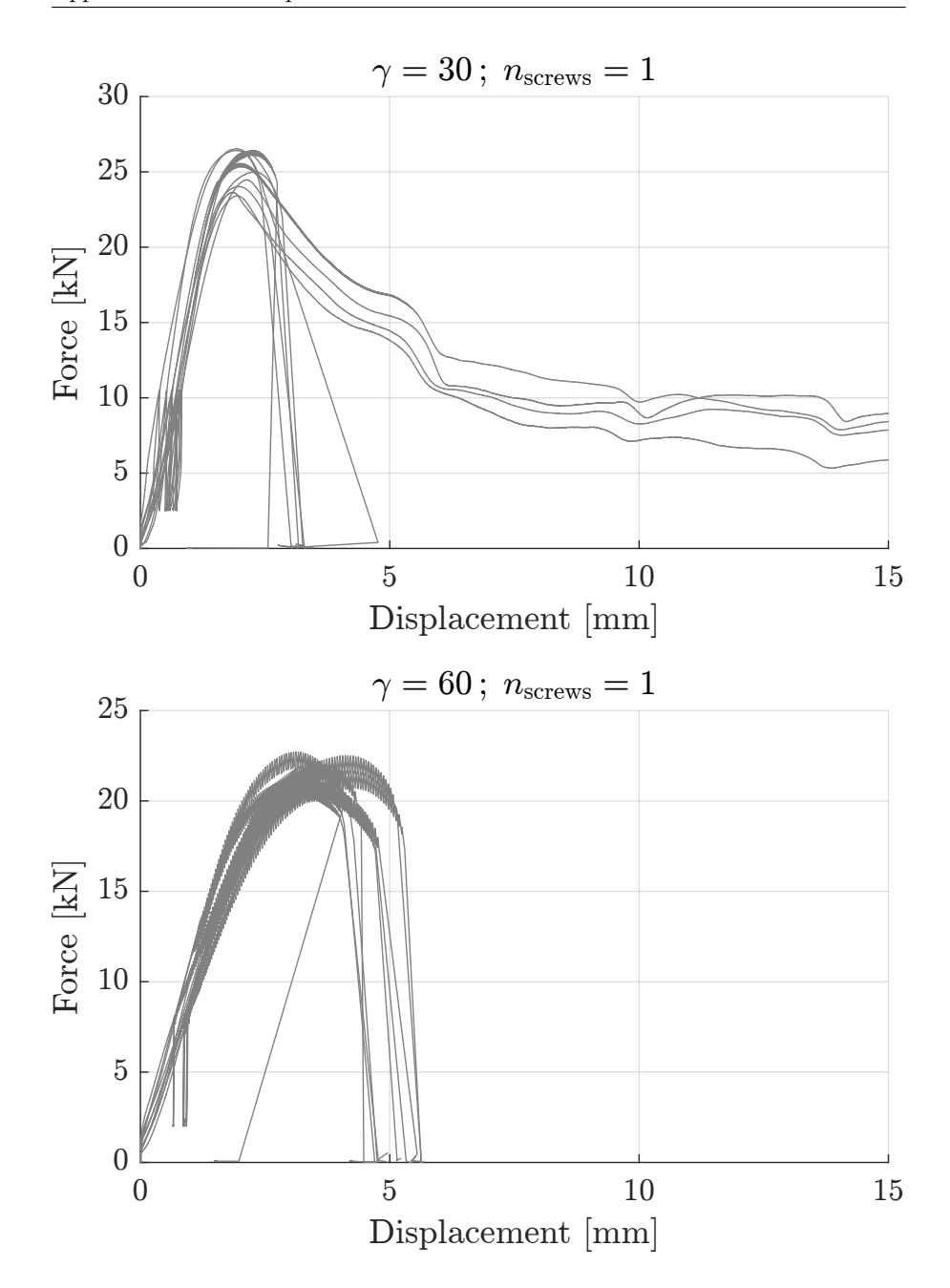
A comprehensive reliability analysis must also include all relevant limit states: beyond bending, shear and axial actions, brittle mechanisms can become governing in joints with many fasteners.

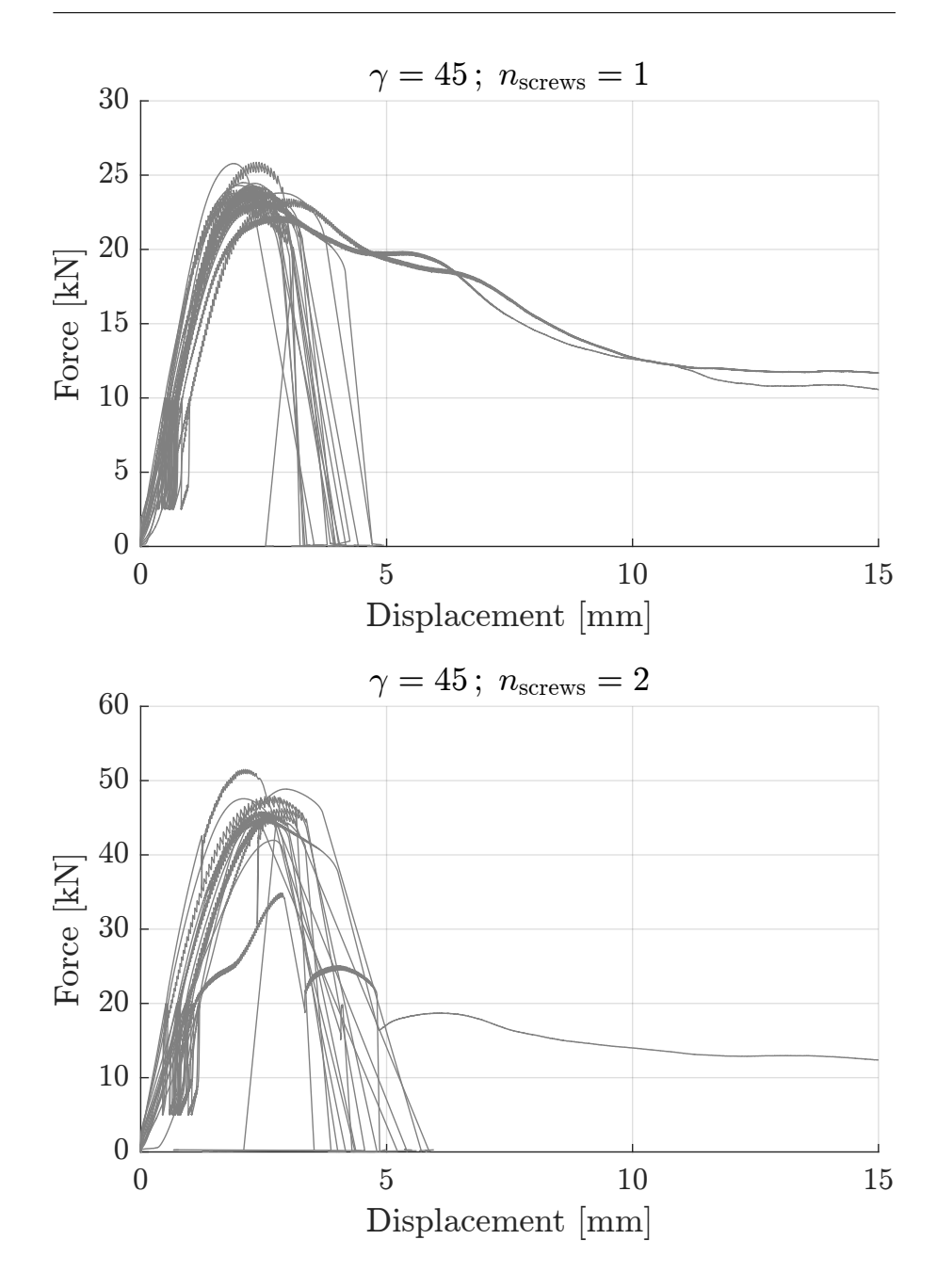
Future work might concern time-dependent variability. Long-term creep, moisture cycling, fatigue and progressive displacement in the joints affect the reliability of the structures.

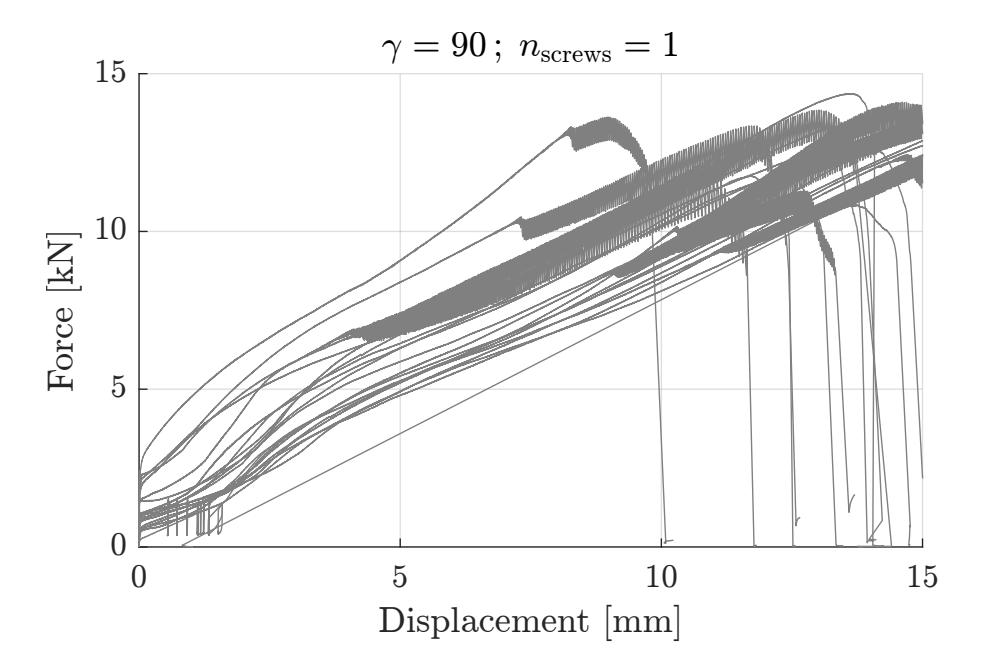
APPENDIX A

Load-displacement curves

The empirical-probabilistic model presented in this thesis was based on single-screw joint test data. Load-displacement curves for double-screw joints were therefore not analysed, but are reproduced here for reference alongside the other datasets of the main test series.







References

- [1] T. E. McLain, "Connectors and fasteners: Research needs and goals," in *Wood Engineering in the 21st Century: Research Needs and Goals*, ASCE, 1998, pp. 56–69.
- [2] AS/NZS 1720.1: Timber structures Part 1: Design methods. Standards Association of Australia, Standards New Zealand, 2022.
- [3] L.-M. Ottenhaus, R. Jockwer, D. van Drimmelen, and K. Crews, "Designing timber connections for ductility A review and discussion," Construction and Building Materials, vol. 304, Art. no. 124621, 2021. DOI: 10.1016/j.conbuildmat.2021.124621.
- [4] E. Frühwald Hansson, "Analysis of structural failures in timber structures: Typical causes for failure and failure modes," Engineering Structures, vol. 33, no. 11, pp. 2978–2982, Nov. 2011. DOI: 10.1016/j.engstruct.2011.02.045.
- [5] D. Caprio, R. Jockwer, and M. al-Emrani, "Reliability of statically indeterminate timber structures: Modelling approaches and sensitivity study," in *Current Perspectives and New Directions in Mechanics, Modelling and Design of Structural Systems*. CRC Press, 2022.
- [6] A. Klasson, R. Crocetti, I. Björnsson, and E. Frühwald Hansson, "Design for lateral stability of slender timber beams considering slip in the lateral bracing system," *Structures*, vol. 16, pp. 157–163, Nov. 2018. DOI: 10. 1016/j.istruc.2018.09.007.

- [7] S. Schilling, "Structural behaviour and reliability of timber trusses with dowelled steel-to-timber connections," Doctoral Thesis, ETH Zurich, 2022. DOI: 10.3929/ethz-b-000538109.
- [8] J. Mack, "The strength and stiffness of nailed joints under short-duration loading," CSIRO, Tech. Rep., 1966.
- [9] J. Ehlbeck and H. Werner, "Untersuchungen über die Tragfähigkeit von Stabdübelverbindungen," Holz als Roh- und Werkstoff, vol. 46, no. 8, pp. 281–288, Aug. 1988. DOI: 10.1007/BF02615055.
- [10] J. Ehlbeck and H. Larsen, "Eurocode 5 design of timber structures: Joints," *International Workshop on Wood Connectors*, pp. 9–23, 1993.
- [11] E. Acler, "Nanyang Technological University Sports Hall Singapore," in *Proceedings of the 23. Internationales Holzbau-Forum IHF*, Garmisch-Partenkirchen, Germany, 2017.
- [12] R. Crocetti, "Large-span timber structures," in *Proceedings of the World Congress on Civil, Structural, and Environmental Engineering*, 2016, pp. 1–23. DOI: 10.11159/icsenm16.124.
- [13] A. Manuello, "Semi-rigid connection in timber structure: Stiffness reduction and stability interaction," vol. 20, Art. no. 2050072, Jun. 2020. DOI: 10.1142/S0219455420500728.
- [14] M. Baravalle and J. Köhler, "A risk-based approach for calibration of design codes," *Structural Safety*, vol. 78, pp. 63–75, Jan. 2019. DOI: 10. 1016/j.strusafe.2018.12.003.
- [15] J. Köhler, A. Leijten, and A. Jorissen, "Uncertainties related to the strength modeling of dowel type fastener connections," in *Proceeding of* the 9th World Conference on Timber Engineering WCTE 2006, vol. 2, Jan. 2006, pp. 1478–1486.
- [16] W. M. Bulleit, "Uncertainty in Structural Engineering," Practice Periodical on Structural Design and Construction, vol. 13, no. 1, pp. 24–30, Feb. 2008. DOI: 10.1061/(ASCE)1084-0680(2008)13:1(24).
- [17] ISO 2394: General principles on reliability for structures. International Organization for Standardisation, 2015.
- [18] Probabilistic Model Code. Joint Committee on Structural Safety, 2006.
- [19] Eurocode basis of structural design, Brussels, Belgium: European Committee for Standardization (CEN), 2002.

- [20] EN 1995-1-1: Eurocode 5: Design of timber structures Part 1-1: General and rules for buildings. Brussels, Belgium: European Committee for Standardization (CEN), Dec. 2010.
- [21] DIN 1052: Entwurf, Berechnung und Bemessung von Holzbauwerken -Allgemeine Bemessungsregeln und Bemessungsregeln für den Hochbau. Berlin, Germany: DIN Deutsche Institut für Normung e.V, 2008.
- [22] SIA 265: Timber structures. Swiss Society of Engineers and Architects, 2012.
- [23] CEN (2003) Minutes of the sixteenth meeting of Document CEN/TC 250/SC 5: N 209. Brussels, Belgium: European Committee for Standardization (CEN), Oct. 2003.
- [24] prEN 1995-1-1: Eurocode 5 Design of timber structures Part 1-1: General rules and rules for buildings. Brussels, Belgium: European Committee for Standardization (CEN), Sep. 2023.
- [25] A. J. M. Jorissen, "Double shear timber connections with dowel type fasteners," Ph.D. thesis, Delft University of Technology, Dec. 1998.
- [26] K. A. Malo, J. Siem, and P. Ellingsbø, "Quantifying ductility in timber structures," *Engineering Structures*, Modelling the Performance of Timber Structures, vol. 33, no. 11, pp. 2998–3006, Nov. 2011. DOI: 10.1016/j.engstruct.2011.03.002.
- [27] R. Jockwer, D. Caprio, and A. Jorissen, "Evaluation of parameters influencing the load-deformation behaviour of connections with laterally loaded dowel-type fasteners," Wood Material Science & Engineering, vol. 17, pp. 1–14, Jul. 2021. DOI: 10.1080/17480272.2021.1955297.
- [28] I. Smith, A. Asiz, M. Snow, and I. Chui, "Possible Canadian/ISO approach to deriving design values from test data," in *Proceedings of the Meeting 39 of Working Commission W18 Timber Structures, CIB-W18, Paper No. 39-17-1*, Florence, Italy, 2006.
- [29] EN 1998-1:2004: Eurocode 8: Design of structures for earthquake resistance Part 1: General rules, seismic actions and rules for buildings. Brussels, Belgium: European Committee for Standardization (CEN), 2004.

- [30] R. Lemaître, J.-F. Bocquet, M. Schweigler, and T. Bader, "Beam-on-foundation modelling as an alternative design method for timber joints with dowel-type fasteners: Part 2: Modelling techniques for multiple fastener connections," in *Proceedings of Meeting No. 6 of the International Network on Timber Engineering Research INTER*, Paper No. 52-7-9, Tacoma, Washington, USA, 2019.
- [31] J. Gauß and U. Kuhlmann, "Consideration of the connection stiffness in design process experimental investigation," in *Proceedings of the World Conference on Timber Engineering WCTE2018*, Seoul, Korea, 2018, Art. no. 7.
- [32] D. Caprio and R. Jockwer, "Regression models for the description of the behaviour of modern timber joints," *Buildings*, vol. 13, no. 11, Art. no. 2693, Nov. 2023. DOI: 10.3390/buildings13112693.
- [33] D. Otero Chans, J. Estévez Cimadevila, and E. Martín Gutiérrez, "Orientation of bars glued on glued laminated products: Parallel vs. perpendicular," *Composites Part B: Engineering*, vol. 62, pp. 97–103, 2014. DOI: 10.1016/j.compositesb.2014.02.028.
- [34] N. Gattesco, A. Gubana, and M. Buttazzi, "Pull-out strength of bar glued-in joints," in *Proceedings of the World Conference on Timber En*gineering, WCTE 2010, Place: Riva del Garda, Italy, Riva del Garda, Trento, Italy, 2010.
- [35] H. J. Blaß and B. Laskewitz, Glued-in rods for timber structures: effect of distance between rods and between rods and timber edge on the axial strength. Karlsruhe, Germany: Versuchsanstalt für Stahl, Holz und Steine, Abt. Ingenieurholzbau, 2001.
- [36] A. Ringhofer, R. Brandner, and G. Schickhofer, "Withdrawal resistance of self-tapping screws in unidirectional and orthogonal layered timber products," *Materials and Structures*, vol. 48, no. 5, pp. 1435–1447, May 2015. DOI: 10.1617/s11527-013-0244-9.
- [37] E. Toumpanaki, A. Gawne, R. Humphreys, and L. Vojnovic, "Effect of moisture and rate of loading in the withdrawal capacity of screws in cross laminated timber," *Structures*, vol. 69, Art. no. 107530, Nov. 2024. DOI: 10.1016/j.istruc.2024.107530.

- [38] R. Brandner, A. Ringhofer, and T. Reichinger, "Performance of axially-loaded self-tapping screws in hardwood: Properties and design," *Engineering Structures*, vol. 188, pp. 677–699, Jun. 2019. DOI: 10.1016/j.engstruct.2019.03.018.
- [39] U. Mahlknecht and R. Brandner, "Block shear failure mechanism of axially-loaded groups of screws," *Engineering Structures*, vol. 183, pp. 220– 242, Mar. 2019. DOI: 10.1016/j.engstruct.2018.12.057.
- [40] T. Joyce and Y. H. Chui, "Group effects in axially loaded self-tapping screw connections," *Engineering Structures*, vol. 251, Art. no. 113537, Jan. 2022. DOI: 10.1016/j.engstruct.2021.113537.
- [41] M. A. H. Mirdad, A. Jucutan, R. Khan, J. Niederwestberg, and Y. H. Chui, "Embedment and withdrawal stiffness predictions of self-tapping screws in timber," *Construction and Building Materials*, vol. 345, Art. no. 128394, Aug. 2022. DOI: 10.1016/j.conbuildmat.2022.128394.
- [42] H. J. Blaß, I. Bejtka, and T. Uibel, Tragfähigkeit von Verbindungen mit selbstbohrenden Holzschrauben mit Vollgewinde, ISBN: 9783866440340 ISSN: 1860-093X, 2006. DOI: 10.5445/KSP/1000004810.
- [43] R. Tomasi, A. Crosatti, and M. Piazza, "Theoretical and experimental analysis of timber-to-timber joints connected with inclined screws," *Construction and Building Materials*, vol. 24, pp. 1560–1571, 2010. DOI: 10.1016/j.conbuildmat.2010.03.007.
- [44] R. Jockwer, R. Steiger, and A. Frangi, "Fully Threaded Self-tapping Screws Subjected to Combined Axial and Lateral Loading with Different Load to Grain Angles," in *Materials and Joints in Timber Structures*, Dordrecht, 2014, pp. 265–272.
- [45] H. Krenn and G. Schickhofer, "Joints with inclined screws and steel plates as outer members," in *Proceedings of the meeting 35 of working commission W18 Timber Structures CIB-W18, paper no. 42-7-2*, Dübendorf, Switzerland, 2009.
- [46] Y. De Santis, A. Aloisio, D. P. Pasca, I. Gavrić, and M. Fragiacomo, "Mechanical characterization of soundproofed inclined screws connections," Construction and Building Materials, vol. 412, Art. no. 134641, Jan. 2024. DOI: 10.1016/j.conbuildmat.2023.134641.

- [47] R. O. Foschi, "Load-slip characteristics of nails," Wood science, vol. 7, pp. 69–76, 1974.
- [48] R. M. Richard and B. J. Abbott, "Versatile elastic-plastic stress-strain formula," *Journal of the Engineering Mechanics Division*, vol. 101, no. 4, pp. 511–515, Aug. 1975. DOI: 10.1061/JMCEA3.0002047.
- [49] P. Glos, "Zur Bestimmung des Festigkeitsverhaltens von Brettschichtholz bei Druckbeanspruchung aus Werkstoff-und Einwirkungskenngrößen," Ph.D. Thesis, Berichte zur Zuverlässigkeitstheorie der Bauwerke, No. 35/78, Technische Universität München, Munich, Germany, 1978.
- [50] R. Brandner, A. Ringhofer, and M. Grabner, "Probabilistic models for the withdrawal behavior of single self-tapping screws in the narrow face of cross laminated timber (CLT)," European Journal of Wood and Wood Products, vol. 76, no. 1, pp. 13–30, 2018. DOI: 10.1007/s00107-017-1226-3.
- [51] G. Flatscher, Evaluation and approximation of timber connection properties for displacement-based analysis of CLT wall systems (Monographic Series TU Graz: Timber Engineering & Technology). Verlag der Technischen Universität Graz, 2017, vol. TET 6.
- [52] D. V. Doyle, "Performance of joints with eight bolts in laminated Douglasfir," U.S. Department of Agriculture, Forest Service, Forest Products Laboratory, Madison, WI, U.S. Forest Service Research Paper FPL 10, Jan. 1964, 36 pp.
- [53] G. Lantos, "Load distribution of a row of fasteners subjected to lateral load," Timber Research and Development Association (TRADA), High Wycombe, United Kingdom, Research Report, 1967.
- [54] G. Lantos, "Load distribution of a row of fasteners subjected to lateral load," *Wood Science*, vol. 1, no. 3, pp. 129–136, 1969.
- [55] C. O. Cramer, "Load distribution in multiple-bolt tension joints," *Journal of the Structural Division*, vol. 94, no. 5, pp. 1101–1117, May 1968.
- [56] M. Schweigler, T. K. Bader, and G. Hochreiner, "Engineering modeling of semi-rigid joints with dowel-type fasteners for nonlinear analysis of timber structures," *Engineering Structures*, vol. 171, pp. 123–139, Sep. 2018. DOI: 10.1016/j.engstruct.2018.05.063.

- [57] T. L. Wilkinson, "Load Distribution among Bolts Parallel to Load," Journal of Structural Engineering, vol. 112, no. 4, pp. 835–852, Apr. 1986. DOI: 10.1061/(ASCE)0733-9445(1986)112:4(835).
- [58] H. Krenn, "Ein Beitrag zur Stahlblech-Holz-Zuglaschenverbindung mit geneigt angeordneten selbstbohrenden Holzschrauben," Institute of Timber Engineering and Wood Technology, Dissertation, Graz University of Technology, 2017.
- [59] J. J. Zahn, "Design Equation for Multiple-Fastener Wood Connections," *Journal of Structural Engineering*, vol. 117, no. 11, pp. 3477–3486, Nov. 1991. DOI: 10.1061/(ASCE)0733-9445(1991)117:11(3477).
- [60] J. Lauritzen Jensen, Dowel-type fastener connections in timber structures subjected to short-term loading: Ph.D.thesis (SBI-report). Hørsholm: SBI forlag, 1994.
- [61] T. Descamps, L. Van Parys, and S. Datoussaïd, "Development of a specific finite element for timber joint modeling," *International Journal for Computational Methods in Engineering Science and Mechanics*, vol. 12, no. 1, pp. 1–13, Jan. 2011. DOI: 10.1080/15502287.2010.540299.
- [62] T. Bader, J.-F. Bocquet, M. Schweigler, and R. Lemaître, "Numerical modeling of the load distribution in multiple fastener connections," in Design of Connections in Timber Structures: A State-of-the-Art Report by COST Action FP1402 / WG3, C. Sandhaas, J. Munch-Andersen, and P. Dietsch, Eds., Aachen: Shaker Verlag, 2018, pp. 221–239.
- [63] Y. De Santis and M. Fragiacomo, "Timber-to-timber and steel-to-timber screw connections: Derivation of the slip modulus via beam on elastic foundation model," *Engineering Structures*, vol. 244, Art. no. 112798, Oct. 2021. DOI: 10.1016/j.engstruct.2021.112798.
- [64] T. K. Bader, H. J. Blaß, J.-F. Bocquet, et al., in Design of connections in timber structures, 2018.
- [65] K.-H. Gotz, D. Hoor, K. Mohler, and J. Natterer, Timber Design and Construction Sourcebook: a comprehensive guide to methods and practise. McGraw-Hill Publisher Company, 1989.
- [66] A. J. M. Leijten, "Requirements for moment connections in statically indeterminate timber structures," *Engineering Structures*, vol. 33, no. 11, pp. 3027–3032, Nov. 2011. DOI: 10.1016/j.engstruct.2011.03.014.

- [67] A. S. Rebouças, Z. Mehdipour, J. M. Branco, and P. B. Lourenço, "Ductile moment-resisting timber connections: A review," *Buildings*, vol. 12, no. 2, Art. no. 240, Feb. 2022. DOI: 10.3390/buildings12020240.
- [68] C. Hein, "Developing hybrid timber construction for sustainable tall buildings," CTBUH Journal, no. Issue III, pp. 40–45, 2014, Includes description of LCT ONE floor system as timber–concrete composite (TCC) slabs.
- [69] W. Sebastian, A. Lawrence, and A. Smith, "Commentary: The potential for multi-span continuous timber-concrete composite floors," *Proceedings of the Institution of Civil Engineers Structures and Buildings*, vol. 171, no. 9, pp. 661–662, Jul. 2018. DOI: 10.1680/jstbu.171.9.661.
- [70] S. Krug, J. Jaaranen, G. Fink, and J. Schänzlin, "Determination of the moment-rotation relation of continuous timber-concrete composite floors based on the component method," *Structures*, vol. 69, Art. no. 107365, Nov. 2024. DOI: 10.1016/j.istruc.2024.107365.
- [71] D. Caprio, "Consideration of the non-linear behaviour of joints for efficient design of complex timber structures," Licentiate thesis, Chalmers University of Technology, 2023.
- [72] J. Chilton and G. Tang, *Timber gridshells: architecture, structure and craft.* Taylor & Francis, 2016.
- [73] B. Sudret and S. Marelli, Lecture Notes on Structural Reliability and Risk Analysis. Zurich, Switzerland: ETH Zurich, 2018, Lecture notes.
- [74] S. Marelli and B. Sudret, "Uqlab: A framework for uncertainty quantification in matlab," in In The 2nd International Conference on Vulnerability and Risk Analysis and Management (ICVRAM 2014), University of Liverpool, United Kingdom, 2014.
- [75] S.-K. Au and J. L. Beck, "Estimation of small failure probabilities in high dimensions by subset simulation," *Probabilistic Engineering Mechanics*, vol. 16, no. 4, pp. 263–277, Oct. 2001. DOI: 10.1016/S0266-8920(01) 00019-4.
- [76] M. Hansson and P. Ellegaard, "System reliability of timber trusses based on non-linear structural modelling," *Materials and Structures*, vol. 39, no. 6, pp. 593–600, Jul. 2006. DOI: 10.1617/s11527-006-9098-8.

- [77] P. H. Kirkegaard, J. D. Sørensen, D. Čizmar, and V. Rajčić, "System reliability of timber structures with ductile behaviour," *Engineering Structures*, vol. 33, no. 11, pp. 3093–3098, Nov. 2011. DOI: 10.1016/j.engstruct.2011.03.011.
- [78] F. Brühl, U. Kuhlmann, and A. Jorissen, "Consideration of plasticity within the design of timber structures due to connection ductility," *Engineering Structures*, vol. 33, no. 11, pp. 3007–3017, Nov. 2011. DOI: 10.1016/j.engstruct.2011.08.013.
- [79] O. Dahlberg and N. Vallström, "Experimental investigation of steel-to-timber joints with inclined self-tapping screws: A parametric study evaluating load-displacement behavior and testing configurations in quasi-static testing," Bachelor Thesis, Chalmers University of Technology, 2024.
- [80] EN 12512: Timber structures: Test methods Cyclic testing of joints made with mechanical fasteners. Brussels, Belgium: European Committee for Standardization (CEN), 2002, Type: Standard.
- [81] ISO 8503-1: Preparation of steel substrates before application of paints and related products Surface roughness characteristics of blast-cleaned steel substrates. International Organization for Standardization, 1988.
- [82] ISO 6892-1: Metallic materials Tensile testing Part 1: Method of test at room temperature. International Organization for Standardization, 2019.
- [83] D. Caprio and R. Jockwer, "Experimental investigation and probabilistic modelling of the load-displacement behaviour of steel-to-timber joints with self-tapping screws," Construction and Building Materials, vol. 489, Art. no. 141970, Aug. 2025. DOI: 10.1016/j.conbuildmat.2025. 141970.
- [84] ETA-11/0190: Self-tapping screws for use in timber constructions. EOTA, 2018.